

Rolled-up Nanotechnology: Materials Issue and Geometry Capability

Changhao Xu, Xiang Wu, Gaoshan Huang, and Yongfeng Mei*

Rolled-up nanotechnology is an appealing technique that tunes planar films into complex 3D fine structures. The rolling-up mechanism and methodology of a huge variety of materials and their combinations are summarized, including metals, insulators, traditional semiconductor families, polymers, and recently emerged 2D materials. The basic principles of strain induction, fabrication methods, and technical aspects of rolled-up nanotechnology are described. The control over the geometry, as well as its deformation, directionality, and chirality are also discussed. Apart from rolling up into tubes or rings, springs, and other 3D complex structures can also be fabricated through this technique. Exploiting novel physical and mechanical properties in these rolled-up structures has recently inspired numerous applications, including optical resonators, energy storage, drug delivery, gas detection, and environmental decontamination. Such widely applicable and highly tunable 3D architectures open up exciting future opportunities for on-chip applications.

1. Introduction

The development of complex 3D micro/nanoarchitectures has sparked enormous research interest due to its potential for advanced electronics,^[1–4] photonics,^[5–11] mechanics,^[12–16] and microelectromechanical systems (MEMS).^[17–20] A number of approaches have been developed to form these 3D architectures, such as 3D printing with polymeric inks,^[21,22] two and multiphoton lithography,^[23–27] large-area projection micro-stereolithography (LAPμSL),^[15,28] and template-assisted deposition^[29,30] (Figure 1). These impressive techniques have offered various manufacturing capabilities with high design freedom and arbitrary critical feature sizes and thus represent an important milestone toward 3D micro/nanoarchitectures. However, most of these techniques fabricate 3D structures from a bottom-up perspective. For instance, two-photon lithography typically begins by fabricating photosensitive polymer-based 3D microstructures, and then covert the materials template to desired materials by exchange growth using atomic layer deposition or

chemical vapor deposition (CVD). When it comes to on-chip integrations, these strategies are limited by accessible materials and slow processing rate,^[31] and the generated defects in the produced amorphous materials placed restrictions to its further applications in high-performance devices.^[32] Therefore, novel approaches and methods of fabricating 3D micro/nanostructures are highly demanded.

Rolled-up nanotechnology is an alternative technique that fabricates 3D nanostructures out of planar films called nanomembranes. Nanomembranes are defined as planar thin films with thicknesses between one to a few hundred nanometers.^[33] These nanomembrane materials behave like soft materials while maintaining excellent properties like their bulk counterpart and therefore is an ideal platform for fabricating 3D nano-

structures. Inspired by concepts of origami and kirigami,^[34–37] researchers folded and rolled these nanomembranes into a number of fascinating 3D structures.^[17,38–44] Several review articles have been published with emphasis on nanomembranes thinning and manufacture, mechanical deformation, fundamental studies, and their practical applications.^[33,41,45–47] By releasing strain-engineered planar functional nanomembranes on sacrificial layers, complex rolled-up structures including tubes,^[48–54] rings,^[54–56] and helices^[42,57–59] can be constructed (for instance, see Figure 1f). This approach can be applied to engineer a wide range of organic and inorganic materials and their combinations, including metals, insulators, traditional semiconductor families, and recently emerged 2D materials. Given its compatibility to standard CMOS fabrication process and ability to manufacture large periodic arrays with precise geometric control, rolled-up nanotechnology further expands the applications of 3D nanostructures to a number of areas, including optical resonators,^[60,61] photodetectors,^[62,63] micro-motors,^[64–66] energy storage,^[67] drug delivery,^[68] gas detection,^[53] and environmental decontamination.^[69] The versatility in the materials design and geometric tuning in rolled-up nanotechnology presents tremendous opportunities for further developing sophisticated 3D fine structures.

In this review, we focus on the materials perspective and fabrication process of rolled-up nanotechnology. First, we give a brief introduction of rolled-up mechanism, as well as its fabrication techniques and control strategies. We summarize and highlight recent advances of different materials systems and their corresponding rolling methodologies. Second,

C. H. Xu, X. Wu, Prof. G. S. Huang, Prof. Y. F. Mei
 Department of Materials Science
 State Key Laboratory of ASIC and Systems
 Fudan University
 Shanghai 200433, P. R. China
 E-mail: yfm@fudan.edu.cn

 The ORCID identification number(s) for the author(s) of this article can be found under <https://doi.org/10.1002/admt.201800486>.

DOI: 10.1002/admt.201800486

the geometry control of the produced structures is discussed, including rolling directionality, tube diameter, and chirality of springs. Third, mesostructures besides microtubes formed utilizing rolling mechanism are discussed and summarized. Finally, we present an outlook on the directions of rolled-up nanotechnology for future on-chip applications.

2. Rolling Mechanism

It is well known in fundamental physics that moment drives a static object to rotate. As the rolling-up process can be considered as the rotation of part of the nanomembranes, there must exists nonzero moment in the membranes system. In terms of rolled-up nanotechnology, the moment comes from either strain relaxation or external forces.^[17,45] In other words, strain relaxation and external force are the driving mechanism for the formation of 3D structures based on rolling-up nanomembranes. Hence, the methods to introduce and manipulate strain gradient perpendicular to the nanomembranes system or external force acting on the membranes are the most essential element and deterministic factor in the rolled-up nanotechnology. Here, we review and classify these methods according to different mechanisms.

2.1. Internal Strain Gradient

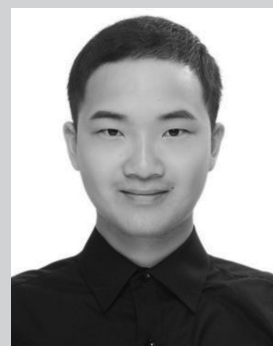
Internal (or intrinsic) strain gradient exists inside the nanomembranes system, and is the most commonly used strain type in rolled-up nanotechnology. The strain gradient is either generated during the deposition of nanomembranes or introduced right before the rolling process. According to different mechanisms, the internal strain gradient can be introduced by the following methods:^[17,45] (a) utilizing lattice mismatch in heteroepitaxial crystalline bilayer, (b) via nonepitaxial deposition methods, (c) utilizing different swelling properties or (d) thermal response properties of different materials, (e) utilizing lattice mismatch resulted from topochemical transformation, or (f) via surface reconstruction of ultrathin nanomembranes. In the following sections, the mechanisms of the above six methods along with the corresponding advantages and disadvantages will be discussed in details with specific examples.

2.1.1. Heteroepitaxial Crystalline Bilayer

The strain gradient in the heteroepitaxial grown bilayer originates from the different lattice constant of different materials.^[17] This method was first reported in 2000,^[70] where epitaxially grown GaAs/InAs bilayer rolled up into microtubes upon the etching of the sacrificial layer (AlAs), as shown in **Figure 2a**. In details, the lattice constant of In is larger than that of Ga. Thus, when a layer of GaAs is epitaxially grown on the crystalline InAs, the upper layer would be stretched in order to fit the lattice constant of the lower layer at the interface, while the lower layer will shrink. In this way, a tensile strain is introduced in the GaAs layer, while the InAs layer is in compression. For such heteroepitaxial crystalline bilayer system, upon strain



Changhao Xu received his B.S. degree in Materials Science from Fudan University, under the supervision of Prof. Yongfeng Mei. He is currently pursuing his Ph.D. degree in Medical Engineering at California Institute of Technology. His research interests include flexible electronics, wearable biomedical devices, and rolled-up nanotechnology.



Xiang Wu is an M.S. student in the Department of Materials Science and Engineering at Stanford University. He received his B.S. in Material Physics at Fudan University in 2018, under the supervision of Prof. Yongfeng Mei. His current research interests focus on photonic devices and materials, optical microcavities, and rolled-up nanotechnology.

relaxation via etching of the sacrificial layer, the upper layer tends to shrink and the lower layer tends to expand, causing a bending moment which eventually results in the rolling up of GaAs/InAs bilayer. Such mechanism can be applied to other epitaxy materials systems, such as SiGe^[48,71] and AlN/GaN.^[72]

2.1.2. Nonepitaxial Deposited Prestrained Nanomembranes

Besides heteroepitaxial grown bilayer, nanomembranes deposited via nonepitaxial methods such as electron beam evaporation, magnetron sputtering, and ion plating can also contain built-in strain gradient even though those nanomembranes are either polycrystalline or amorphous.^[17,41,51] Cr deposited by electron beam evaporation is a commonly used strained metal nanomembrane,^[73–75] and is often incorporated with semiconductor layers. For example, researches have shown that the Cr layer deposited onto silicon is highly tensile strained.^[73] Figure 2b,c presents a Cr/SiGe-on-insulator system fabricated via Ge condensation.^[75] Once the top Cr/SiGe bilayer is released from the substrate via selective etching, the Cr layer and the SiGe layer would relax inward and outward, respectively, resulting in a bending moment that causes the bilayer to roll upward. Furthermore, the strain gradient inside the Cr layer can be controlled by the evaporation rate.^[17] It should be noted that as the bending moment linearly depends on the distance between the mean positions of the forces applied to the upper and lower layers,^[76] the rolling process of nanomembranes system also depends on the thickness of Cr layer, and

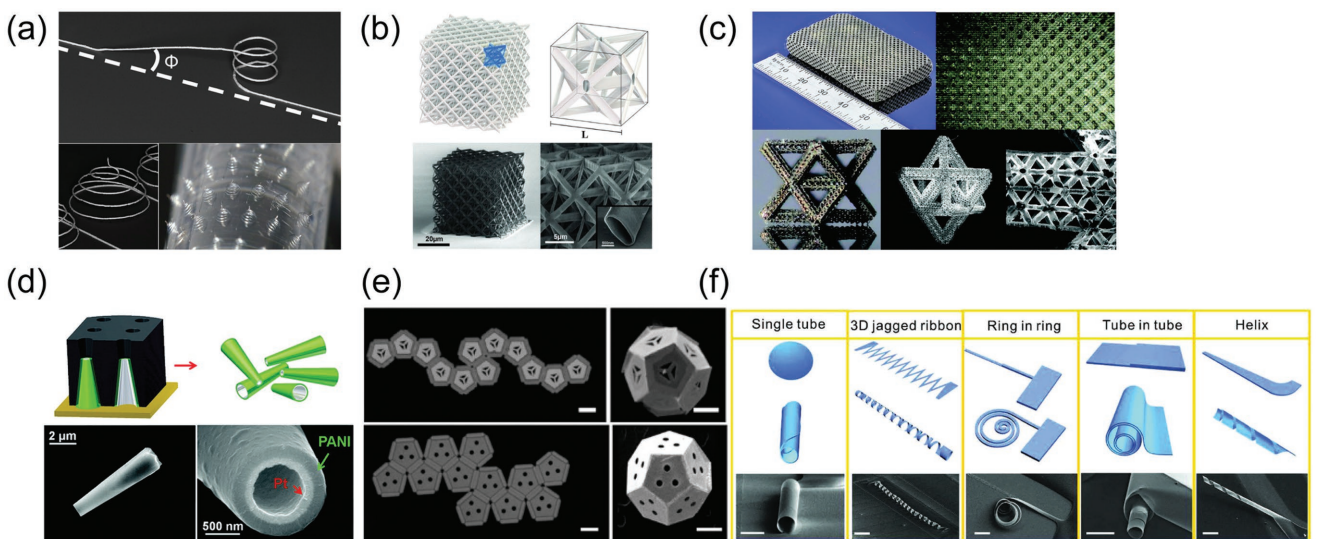


Figure 1. Fabrication methods of 3D micro/nanoarchitectures. a) 3D-printed helices and hemispherical spiral array. Adapted with permission.^[21] Copyright 2016, National Academy of Sciences. b) Architecture and microstructure of nanolattices using two-photon lithography. Reproduced with permission.^[12] Copyright 2014, AAAS. c) Hierarchical metamaterial and critical features fabricated by LAPμSL. Adapted with permission.^[15] Copyright 2016, Macmillan Publishers Limited. d) Template-assisted electrodeposition of microtubes. Adapted with permission.^[29] Copyright 2011, American Chemical Society. e) Self-folded 3D structures (scale bars: 300 μm). Adapted with permission.^[34] Copyright 2011, National Academy of Sciences. f) Rolled-up 3D mesostructures (scale bars: 10 μm). Reproduced with permission.^[54] Copyright 2017, Wiley-VCH.

the Cr layer below a certain critical thickness could not exert a torque large enough to induce the rolling-up process.^[75] Moreover, such prestrained nanomembranes deposited by nonepitaxial methods are not restricted to metal films.^[17] Insulators, such as Si_xN_y , are also widely used as a strained layer.^[73,77,78] Depending on the deposition parameters, the strain inside Si_xN_y can be either compression or tension. For example,

a 10 nm thick Si_xN_y layer deposited by low-pressure CVD (250 mTorr) at 800 °C from a dichlorosilane/ammonia gas mixture with a growth rate of 3.5 nm min⁻¹ exhibits a considerable residual tensile strain,^[73] while the Si_xN_y film obtained under similar conditions except higher pressure (600 mTorr) presents a compressive strain.^[79] The microtube fabricated with the aid of Si_xN_y strained layer is shown in Figure 2d.

The advantages of the above mentioned methods are obvious: nonepitaxial deposition methods exhibit a significant reduction in cost when compared with epitaxial methods. However, this way of introducing internal strain requires a layer of strained nanomembranes besides the functional material. The existence of strain layer might influence the characterization of the functional layer, or even erode its properties, limiting the usage of this method. To overcome this problem, strained single-layer nanomembranes were introduced by changing the deposition parameters during growth, such as the substrate temperature and growth rate, and no additional prestrained layer is needed.^[51] The mechanism behind this method can be simplified and explained by a bilayer model. The single-layer system could be regarded as a bilayer with equal thickness, and the properties of the two layers are different due to discrepancy in deposition parameters, leading to a strain difference between the two layers. Take the deposition rate as an example, if the bottom layer and the top layer are deposited at different rates, the grain sizes in the two layers would be different, exerting different stress levels in the nanomembranes.^[80]

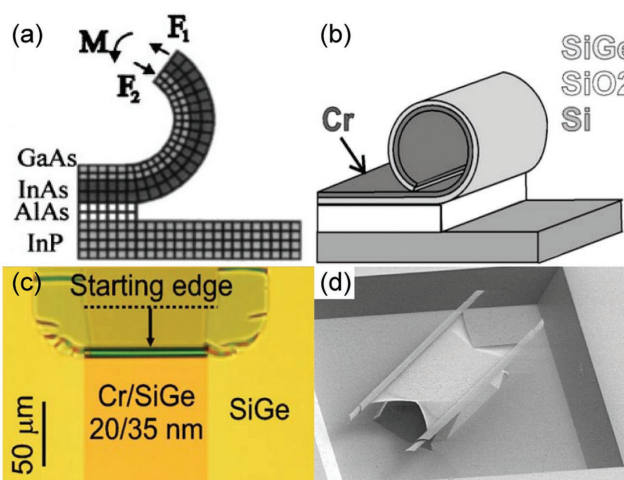


Figure 2. a) Schematic diagram showing the mechanism of introducing strain gradient in heteroepitaxial crystalline bilayer. Reproduced with permission.^[70] Copyright 2000, Elsevier. b) Schematic diagram illustrating the rolling-up process of the Cr/SGOI nanomembranes system. c) Optical microscopy showing the rolled-up microtubes utilizing Cr as the strained layer. (b,c) Reproduced with permission.^[75] Copyright 2008, American Institute of Physics. d) SEM image of two suspended SiGe/Si/Si₃N₄/Cr (10/10/10/18 nm) microtubes with a diameter of 3.8 μm . Reproduced with permission.^[73] Copyright 2004, American Institute of Physics.

2.1.3. Swelling Strain

Unlike the above mentioned two methods which introduce strain during the deposition of nanomembranes, the strain can

also be generated inside membranes system upon the change in environment. In the case of swelling strain, the rolling process is not confined to inorganic materials. Strain can also be introduced in organic membranes system and microtubes can also be formed utilizing different swelling properties of chemically dissimilar polymers in selective solvents.^[49] **Figure 3** demonstrates a bilayer polymer system which consists of polystyrene (PS) and poly(4-vinylpyridine) (P4VP). PS forms a stiff hydrophobic layer upon exposure to water due to its low water uptake, while P4VP is less hydrophobic and thus swells in acid aqueous solutions. When putting the bilayer system into contact with acid aqueous solutions, the two layers present an unequal change in volume, resulting in the lateral forces which eventually create the bending moment for rolling process. Recently, such approach has also been widely applied to the construction of 4D mesostructures.^[81]

2.1.4. Thermal Response Strain

Similar to swelling strain, thermal response strain is also generated upon the change of environment parameters, and in the case of thermal response strain, the parameter is temperature.^[17,41] The mechanism behind the thermal response strain lies in the different thermal properties of different materials, and the most straightforward way is to utilize the discrepancy in coefficient of thermal expansion (CTE). The classical example of utilizing CTE in macroscale world is the bimetallic strips in thermostats.^[17] As the temperature changes, the two metal layers shrink or expand to different extents due to the discrepancy in CTE, resulting in thermal induced strain between the metal interface which eventually leads to the bending of the bilayer. The same mechanism can be applied to microscale world and introduce strain in nanomembranes system.^[82] As shown in **Figure 4a**, the top Si layer of silicon-on-insulator (SOI) wafer was first patterned into ribbons via photolithography and reactive ion etching. Then a layer of polydimethylsiloxane (PDMS) was elastically stretched by heating from 30 to 180 °C. Then the stretched PDMS was brought into conformal contact with the Si ribbons. As the CTE of PDMS is approximately two orders of magnitude larger than that of Si,^[17] when the PDMS was released to its unstrained state by cooling, surface deformation of Si was simultaneously formed which caused well-defined waves in Si ribbons with decent uniformity.

Apart from utilizing thermal response strain via changing the environment temperature or thermal heating, there is another way to change the temperature of the certain part of the membranes system—electron beam irradiation,^[83] which is available in transmission electron microscopy (TEM). It is well known that electron beam irradiation would cause the excitation of phonons which leads to the heating of nanomembranes. The heating effect of electron beam irradiation has been utilized to induce the curling and closure of graphitic networks.^[84] More recently, carbon-based nanocomposite tubular structures have been created utilizing electron beam irradiation.^[85] As shown in **Figure 4b**, an opening is made on a carbon nanomembrane with a thickness of 10 nm and the nanomembrane is then exposed to irradiation by an electron beam. The carbon nanomembrane gradually rolled up into tubular nanostructures. The mechanism behind the rolling process could be explained as following: the electron beam irradiation effectively heated the carbon film, leading to a temperature difference between the membrane and the substrate. Such temperature discrepancy results in the strain gradient that eventually causes the rolling of carbon films.^[84,85] Furthermore, other nanostructure such as nanoparticles, nanorods, nanowires, and nanosheets could be loaded on the carbon nanomembrane to form hybrid tubular structures. Moreover, it should be noted that heating via electron beam irradiation does not exhibit the same effect as thermal heating, as irradiation may render other influence to the nanomembranes such as knock-on atom displacements, defects, and self-organization phenomenon.^[83]

2.1.5. Topochemical Transformation Strain

Similar to the strain in heteroepitaxial crystalline bilayer, the topochemical transformation strain is also generated utilizing lattice mismatch. However, to the best of our knowledge, this method has only been reported once utilizing a specific topochemical transformation,^[86] in which a 2D material was rolled up into microtubes. As shown in **Figure 4c**, the CaF₂ nanosheets with the thickness of 1–2 unit cells react with lanthanum salts in water at ambient conditions, causing a topochemical conversion to yield partially oxidized lanthanum fluoride nanosheets. The strain generated from the lattice mismatch produced by this transformation induces the spontaneous rolling-up process of LaF_{3-x}O_x nanosheets.

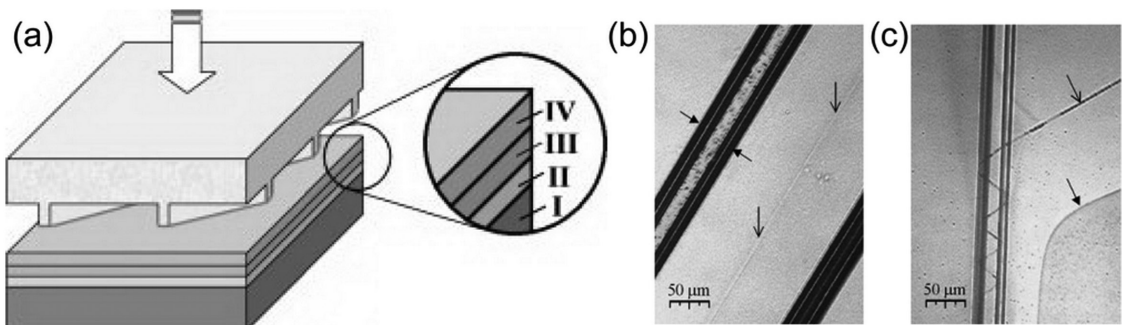


Figure 3. a) Schematic diagram showing the fabrication process of polymer microtubes with structured inner surface. b) Optical image during the rolling of the tubes. c) Optical image of a transparent polymer microtube with visible inner structure. Adapted with permission.^[49] Copyright 2005, Wiley-VCH.

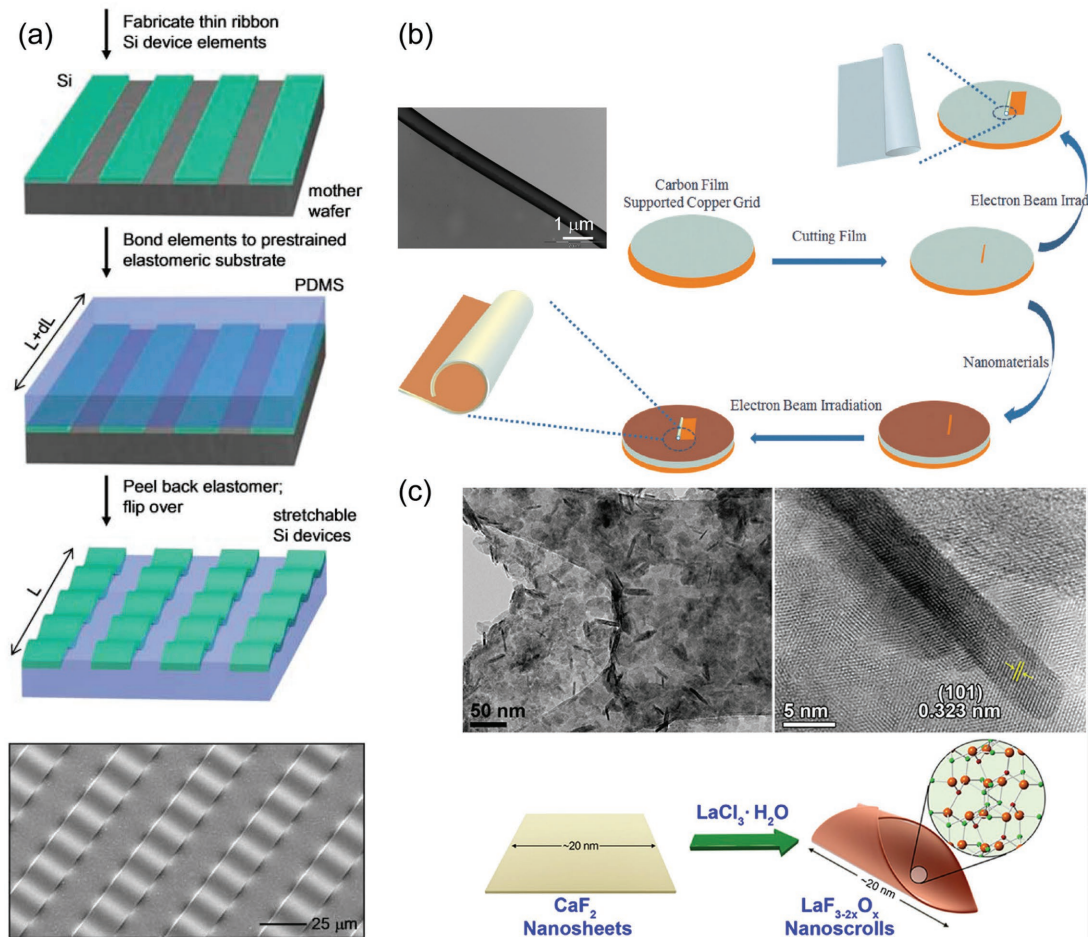


Figure 4. a) Schematic diagram illustrating the fabrication process of wavy Si ribbons utilizing different CTE between PDMS and Si, and SEM image showing the top view of wavy Si ribbons. Adapted with permission.^[82] Copyright 2006, AAAS. b) Schematic illustration of carbon-based nanomembranes rolling up into microtubes under the electron beam irradiation. The inset shows a typical rolled carbon film under the electron beam irradiation of TEM at 100 kV with 1 s duration. Adapted with permission.^[85] Copyright 2012, American Chemical Society. c) Schematic of the overall scrolling process, and TEM image of the $\text{LaF}_{3-x}\text{O}_x$ nanosheet and a single nanotube showing lattice fringing with a d -spacing of 3.23 \AA that matches the (101) plane of the LaF_3 . Reproduced with permission.^[86] Copyright 2016, American Chemical Society.

2.1.6. Strain from Surface Reconstruction

As mentioned in Section 2.1.1, the lattice mismatch strain totally depends on the type of materials under nondefect situation. However, theoretical study has shown that when the thickness of nanomembranes reduces to atomic scale, the intrinsic surface stress caused by surface reconstruction has to be taken into consideration.^[87] Take a Si (001) nanomembrane with a thickness of a few atomic layers as an example. It is well known that the Si (001) surface displays a (2×1) -type reconstruction including rows of dimers.^[88] In an even-layer nanomembrane where the dimers on the top and bottom surface are parallel, the two intrinsic surface stress cancel out with each other. However, in an odd-layer nanomembrane, the dimers on the top and bottom surface are perpendicular, resulting in a surface-stress imbalance which could serve as a driving force for the rolling process. Additionally, it should be noted that the magnitude of such imbalance is considerably large and might even reverse the rolling direction determined from lattice constant.^[87] As

mentioned above, the heteroepitaxially grown Si/Ge bilayer would roll up toward Si according to their lattice constants. However, depending on the orientation of dimers, the surface stress of ultrathin Si/Ge might act along or against the lattice mismatch strain. In the former case, the rolled-up microtube would exhibit smaller diameters, while in the latter case the nanomembrane would roll in the opposite direction. Though discussion about the feasibility of realizing such method experimentally has been proposed,^[89,90] due to its extreme complexity, only theoretical simulation has been reported so far.

2.2. External Force

To the contrary of internal strain gradient, external force does not exist inside the nanomembranes and only acts on the surface of the nanomembranes system. Though not as widely used as internal strain gradient, external force also plays an important role in rolled-up nanotechnology via enhancing or

manipulating the total strain gradient, or inducing the rolling process of specific types of materials. In general, external force could be applied to the nanomembranes system in the following ways: (i) via surface tension of liquid, (ii) utilizing surface adsorption, (iii) via van der Waals force, and (iv) utilizing ultrasonication treatment. In the following sections, the mechanism of the above four methods will be explored in details together with specific examples.

2.2.1. Surface Tension of Liquid

Surface tension is an important property of liquid and could be used to assist or induce the rolling process of nanomembranes. Take liquid droplet as an example, the droplets have a tendency to minimize its surface area (also known as capillary), and such tendency leads to the surface tension between the droplets and the nanomembranes. Surface tension of metal droplets has been reported to assist the rolling up of nanomembranes into microtubes with ultrahigh aspect ratio.^[52,91] As shown in Figure 5a a thin layer of gold (<10 nm) was deposited on the top of prestrained bilayer nanomembranes. After the rapid thermal annealing (RTA) treatment of the sample in N₂ environment, the gold layer formed separated islands due to dewetting. The surface tension between the gold droplets and nanomembranes, together with the intrinsic strain relaxation in the nanomembranes eventually induced the rolling process of nanomembranes. The microtubes fabricated by this method exhibited smaller diameters than the tubes produced via pure intrinsic strain relaxation.^[52] Furthermore, the surface strain of gold droplets could be controlled by their sizes, which could be tuned by the annealing time and temperature. Though in this case the surface tension alone could not induce the rolling of nanomembranes, it should be noted that the surface tension of droplets still brings localized elastic deformation of a

flexible nanomembrane.^[92] Additionally, the surface tension in the grain coalescence of nanodroplets could also be triggered by plasma etching, in which the extent of strain could be controlled by etching times.^[93] Other 3D nanostructures in sub-micrometer scale such as wrinkling, saddling, wedging, and polyhedra shapes have been fabricated utilizing the surface tension of solder droplet, as shown in Figure 5d.^[35,94]

Apart from liquid droplet, the surface tension of solution might also act as the driving force for the rolling-up process of thin-film materials.^[95–97] For example, PDMS sheet, as well as silicon films could be assembled with the assistance of water droplet.^[98,99] Likewise, graphene was reported to roll up into carbon nanoscrolls with the assistance of surface tension of isopropyl alcohol (IPA).^[97] Monolayer graphene was fabricated by mechanical exfoliation of natural graphite on Si wafer with 285 nm SiO₂ top layer. When the chip was immersed into IPA solution for around 5 min and then dried with nitrogen, carbon nanoscrolls were found. The driving force for the rolling up of graphene is actually the surface tension: as the upper and lower surfaces of graphene were in contact with IPA and SiO₂, respectively, the two surfaces experienced different forces. The difference of surface tension resulted in a total surface strain which eventually caused the graphene to roll up upon releasing from the SiO₂. It should be noted that the mass of graphene is extremely low, making it quite sensitive to surface tension, similar to the case of surface reconstruction discussed above.

Additionally, nanomembrane fabricated via chemical synthesis could also be rolled by utilizing surface tension at the air–solution interface.^[100,101] For example, treating the NaAsS₂ solution with a mixture gas flow of HCl and air, and As₂S₃ microtubes with diameters ranging from 20 to 100 μm would form after drying. The mechanism behind the rolling-up process could be explained as following:^[101] as the reaction product—As₂S₃ nanomembrane—is hydrophobic and does

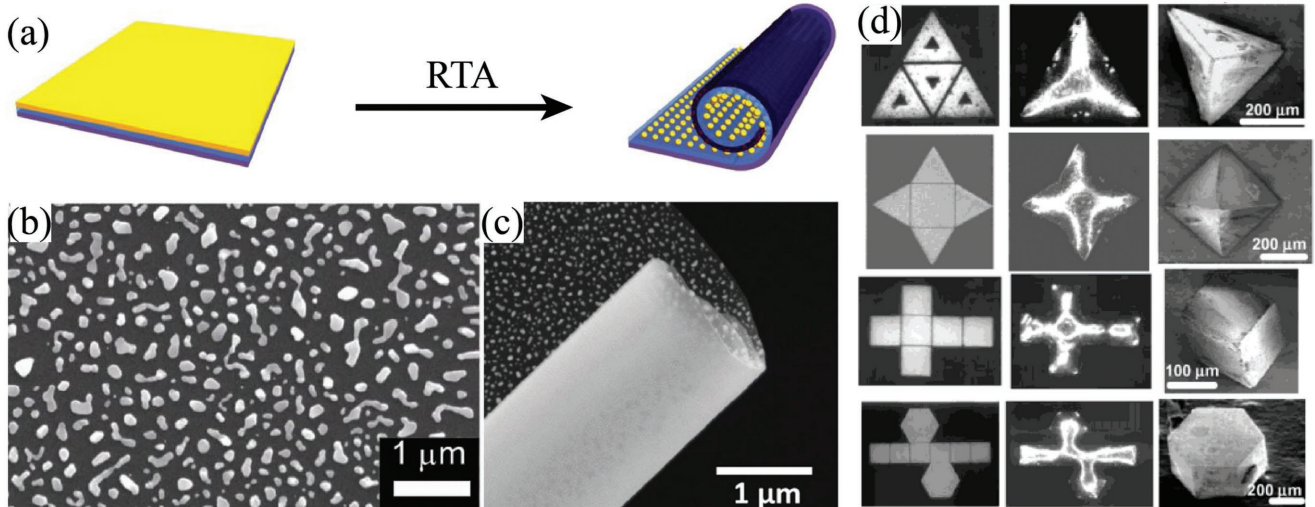


Figure 5. a) Schematic diagram showing the rolling process of nanomembranes with the aid of surface stress from gold droplets. b) SEM image of the surface morphology and c) rolled-up SiO/Si (5/5 nm) microtubes after RTA treatment. (a–c) Adapted with permission.^[52] Copyright 2013, Wiley-VCH. d) Optical microscopy and SEM image of the 2D precursors and polyhedra fabricated by utilizing surface tension of solder. Reproduced with permission.^[35] Copyright 2002, Wiley-VCH.

not sink in the solution, the nanomembrane would exist at the interface of air and solution. During the drying process, the surface tension at the air–layer interface exhibits a larger value than at the side of layer–solution interface. Thus, such imbalanced surface tension leads to the rolling-up process of As_2S_3 film.

2.2.2. Surface Adsorption

It has long been known that surface adsorption could induce the bending of thin films.^[96] If the molecular coverage remains constant, the thinner the film is, the larger the bending curvature will be.^[102] Thus, when reducing the thickness of films to extreme small values, for example, one atomic layer, the surface adsorption might even induce the rolling process of the films. Based on such deduction and using first-principles and classical molecular dynamics simulations, a novel method for fabricating carbon nanotubes utilizing the rolling process of graphene ribbons via surface adsorption of atoms was proposed over a decade ago.^[102,103] In the work of Yu and Liu, H atoms of 50% coverage are randomly adsorbed onto the surface of graphene nanoribbon.^[102] The surface stress induced by adsorption eventually leads the graphene ribbon to roll downward and form a nanotube. The generation of the surface stress could be explained by the following mechanism:^[102] the adsorption of H to the top of a C atom leads to a transition of the bonding configuration of the C atom underneath H from sp^2 to sp^3 . Such transition pulls this C atom up by $\approx 0.3 \text{ \AA}$, while its three neighboring C atoms are pushed out and down, resulting in a tensile stress in the graphene nanoribbon. Calculations also showed that the induced stress increases linearly with the H coverages, and so does the bending curvature. Additionally, it should be noted that other atoms such as F could also be used to trigger the rolling process. Furthermore, the feasibility of this method has recently been justified in experiments,^[104] in which graphene rolled up into tubes under hydrogen and nitrogen atmosphere.

2.2.3. Van der Waals Force

Though relatively weak when compared with ionic or covalent bonds, van der Waals force—the distance-dependent interactions between nanoscale particles—still exerts significant influence on ultrathin films and might even induce the rolling process of some 2D materials. Theoretical works have shown that the van der Waals force between silicon nanowires and graphene nanoribbons could cause the rolling process of graphene.^[105] As shown in Figure 6a, the graphene nanoribbons were put in vicinity of Si nanowire with a distance about 5 Å. Due to the van der Waals force between the nanowire and the nanoribbon, the two start to approach each other. During that process, the carbon atoms near the nanowire begin to wrap on it and the nanoribbon eventually rolls around the whole nanowire, forming a silicon/graphene core–shell structure. It should be noted that the diameter of nanowire plays an important role in this process and only nanowire with the diameter exceeding a certain threshold value could induce the rolling of graphene.^[105]

Though this method has not been experimentally proven, similar method utilizing van der Waals force in a relatively larger scale was demonstrated recently.^[106] As shown in Figure 6b, the nanomembrane floating on the surface of deionized water was approached and gently attached to a tubular substrate by van der Waals adhesion. Afterward, the gradual rotation of the substrate led to the rolling up of the nanomembrane into tubes. It is possible for the fabricated tubes to be damage-free given the low viscosity of water. The rolling-up process of nanomembrane is governed by the competition between the van der Waals force at the substrate–nanomembrane interface and the nanomembrane–water interface.^[106] Various materials including Au, PS, and graphene could be rolled up utilizing this method, and the parameters (such as the winding number and the diameter) of the tubes could be precisely controlled by the rotation of the substrate. Furthermore, freestanding tubes can be produced by pulling out heat-shrink tubular substrate upon

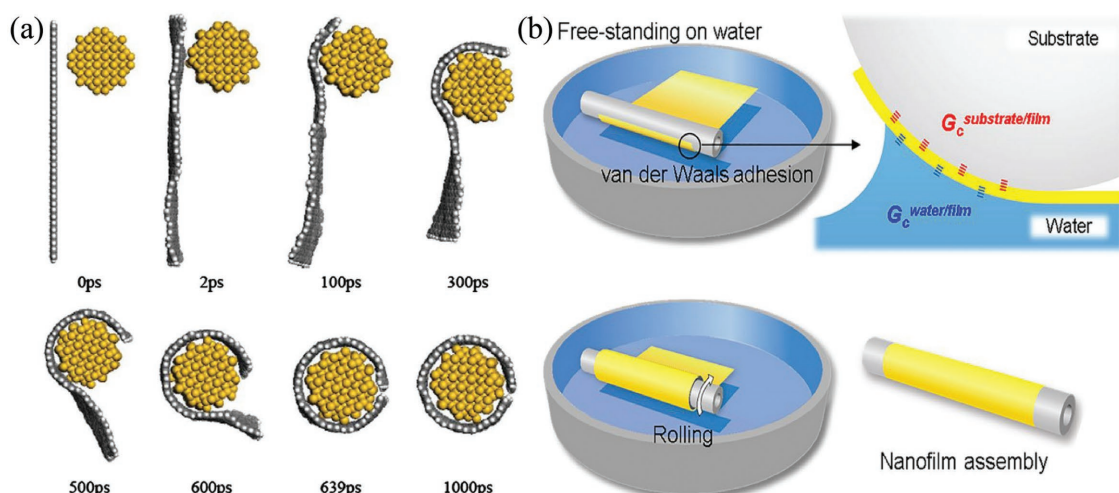


Figure 6. a) The illustration of rolling process of graphene nanoribbon ($33.4 \times 76.6 \text{ \AA}$) onto the Si nanowire (10 \AA in radius) in the simulation. Reproduced with permission.^[105] Copyright 2010, Elsevier. b) Schematic diagram showing the rolling process of nanomembrane floating on water with the aid of tubular substrate. Adapted with permission.^[106] Copyright 2018, American Chemical Society.

heating. However, it should be noted that the diameters of the tubes lie in sub-micrometer scale and tubes with smaller diameters fabricated via this method have not been reported yet.

2.2.4. Ultrasonication Treatment

Applying sound energy to the nanomembranes system, also known as ultrasonication treatment, would also induce the rolling process of some 2D materials.^[103] It has been reported that graphene would form into carbon nanoscrolls upon ultrasonication treatment.^[107] In details, as shown in Figure 7a, graphene was first prepared via wet chemical technique with a donor-type graphite intercalation compounds KC_8 , which reacted exothermically with ethanol, resulting in the formation of exfoliated graphite sheets. Upon sonication, such graphene sheets would roll up into carbon nanoscrolls with a converting rate over 80% (Figure 7b). It should be noted that for efficient formation of such 3D structures, the duration time of the sonication treatment must be short and its energy must be high.^[107]

However, as KC_8 is highly reactive toward oxidants and water vapors in air, such method requires inert atmosphere,^[107,108] such as helium. Acceptor-type graphite intercalation compounds (such as graphite nitrate and hydrosulfate) proposed later might solve this problem.^[109] The overall process is shown in Figure 7c, and ultrasonication treatment is still a must for the formation of carbon nanoscrolls. Additionally, other 2D materials such as graphene oxide have also been rolled up into nanotubes or nanoscrolls via ultrasonication treatment.^[110,111]

3. Release Methods

The fabrication process of rolled-up nanotechnology generally requires a detach procedure to release the obtained

nanomembranes from their substrate in order to shape them into 3D architectures. To release the film, strain-engineered nanomembranes need to be first isolated and shaped. The simplest method is mechanical scratch using a diamond cutter or a piece of sand paper.^[112] As for sophisticated devices that requires a good precision, photolithography or e-beam lithography is intensively used. Detailed shaping methods have been described in the previous review.^[41]

3.1. Wet Release

In most cases, researchers insert a sacrificial layer between the nanomembranes and the substrate to release the wanted nanomembrane from its bulk. Lateral etching of the sacrificial layer separates the freestanding nanomembrane and therein yields the rolled-up process.

According to Mei et al.,^[113] the etching rate of a selected etchant to the sacrificial layer should be 1000 times higher than the dissolving rate of the functional layer. This etching selectivity requirement of the sacrificial layer as to the desired materials need to be considered thoroughly before practical experimentation. Here, we summarize some representative materials systems that have been exploited for fabricating rolled-up nanostructures.

3.1.1. Epitaxially Grown Materials

Group III–V Semiconductors: Wet chemical etching of the sacrificial layer is traditionally adopted since it is cheap and convenient. Rolled-up microtubes were first fabricated by releasing strained InAs/GaAs bilayer with AlAs underneath layer.^[70] In this case, dilute HF solution was applied to remove the AlAs sacrificial layer selectively.^[70,114] Since then various geometries

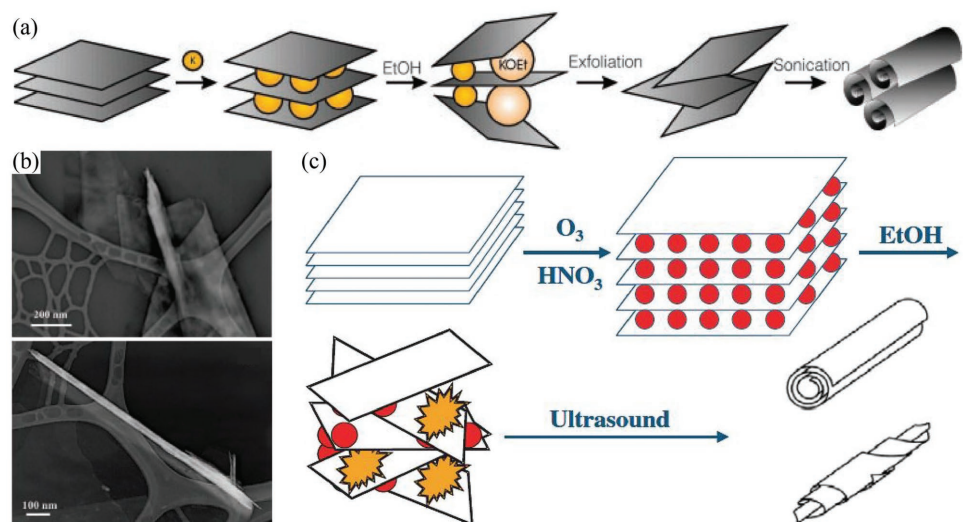


Figure 7. a) Illustration of graphene intercalation, exfoliation, and rolling-up process of graphene with the KC_8 as the intercalation compound. The rolling-up process is triggered by ultrasonication treatment. b) SEM images of carbon nanotubes fabricated by this method. (a,b) Reproduced with permission.^[107] Copyright 2003, AAAS. c) Schematic diagram showing the fabrication process of carbon nanotubes using acceptor-type graphite intercalation compounds. Reproduced with permission.^[109] Copyright 2007, Elsevier.

and studies of GaAs/In_xGa_{1-x}As nanomembranes using the molecular beam epitaxy (MBE) method on GaAs bulk substrate were carried out.^[55,57,115–118] These rolled-up structures were proposed to function as artificial bacterial flagella,^[57] quantum-dot integrated optical resonators,^[119–121,72,115] electromechanical sensors,^[116] and microfluidic devices.^[117]

Group IV Semiconductors: Si/SiGe and SiN_x nanomembrane with Ge sacrificial layer can be released in a H₂O₂ solution at 90 °C.^[122–128] In addition, it was found that the etching rate of heavily boron-doped silicon with a B concentration of 10²⁰ cm⁻³ is 1/8000 that of undoped silicon.^[17] The etching rate of SiGe is even smaller in NH₄OH solution.^[17,129] Hence, researchers released heavily doped Si/SiGe nanomembrane with undoped Si as the sacrificial layer.^[56,74,116,130–132]

Since the component and strain in single-crystal nanomembrane can be well manipulated, the most attractive advantage of MBE grown nanomembranes is its high quality^[133,134] and precise controllability.^[135–137,124] As the lattice constants of commonly used semiconductors have been accurately measured, the strain values in certain heteroepitaxial crystalline bilayer can be precisely identified.^[138,139] For example, under the ideal case where a monocrystalline Ge is epitaxially grown onto a Si (001) substrate without any defects, the misfit strain created at the interface of the bilayer is 4%.^[17] As for compound semiconductors, the lattice constant can be tuned by the composition, and so does the strain value.^[41] An excellent example utilizing such advantage of compound semiconductors is SiGe system, in which the Ge condensation technique provides a decent approach to manipulate the composition and the strain gradient.^[140–142] As shown in Figure 8a,^[141] first, a strained

Si_{1-x}Ge_x layer is epitaxially grown on the SOI wafer. The Ge content in the original SiGe layer is very low but the thickness is much greater than Si. Afterward, the sample is oxidized at a temperature higher than 1000 °C. During the oxidation, the Ge atoms are rejected from the SiGe-oxide layer and also blocked by the bottom oxide layer, thus condensed in Si, forming a SiGe layer between two SiO₂ layers. Eventually, after removing the top oxide layer via HF solution, a layer of Si is epitaxially grown on the SiGe layer, forming a strained Si/SiGe bilayer. The strain value inside the bilayer system depends on the Ge content and distribution in SiGe layer, which can be tuned by the Ge content and thickness of the original SiGe layer, while the oxidation time also plays an important role in determining the strain values.^[141]

However, there are several drawbacks of this method. Primarily, the above discussion about the controllability of strain values in heteroepitaxial crystalline bilayer bases on the prerequisite that the nanomembranes are defect-free. However, nanomembranes with a thickness larger than the thermodynamic critical thickness of plastic relaxation are no longer coherent and would plastically relax through defects. To make the situation even more complicated, the critical thickness does not only depend on the material itself, but also relies on the thickness of the substrate.^[17] In this case, the calculation of strain values only based on lattice constant is actually incorrect. Furthermore, the epitaxial growth of the materials constrains its range to inorganic semiconductors. It is not applicable to other materials such as organics. Additionally, epitaxial growing methods, such as ultrahigh-vacuum MBE and CVD, are extremely expensive, and thus are only confined to a few high-tech laboratories in the world.

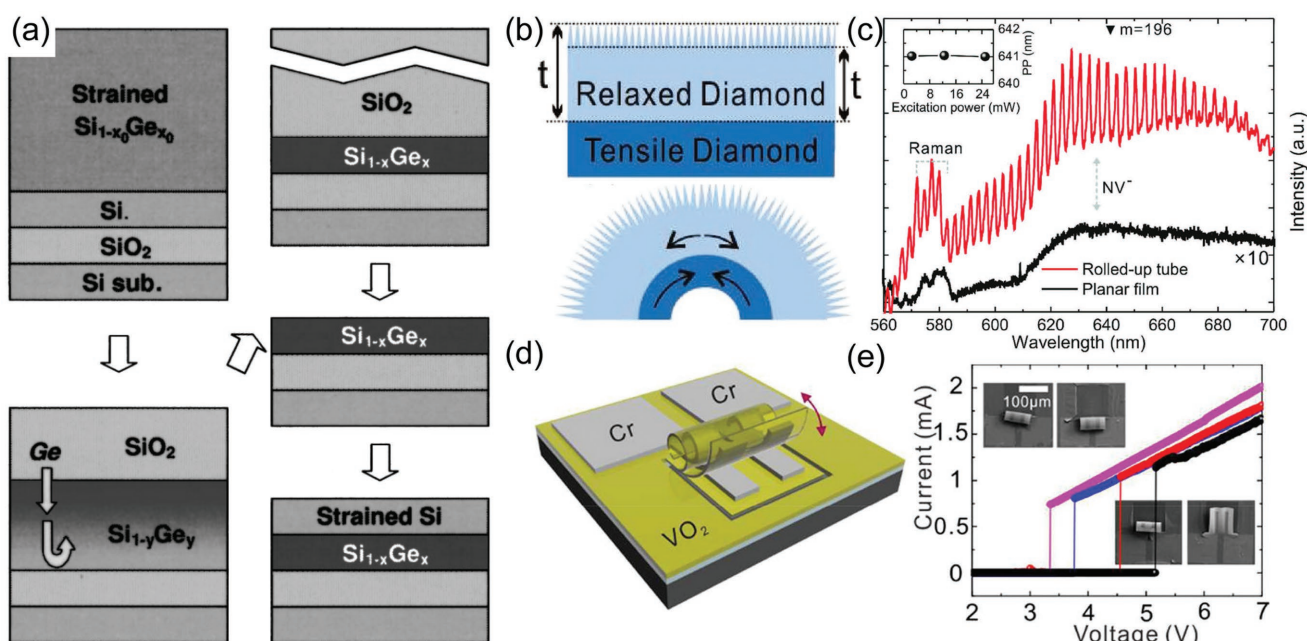


Figure 8. a) Fabrication process of crystalline strained Si/SiGe bilayer via Ge condensation technique. Adapted with permission.^[141] Copyright 2001, American Institute of Physics. b) Schematic of an inverted rolling-up process of nanocrystalline diamond nanomembrane. c) PL spectra of a planar nanocrystalline diamond film (black line) and a rolled-up tube (red line). (b,c) Reproduced with permission.^[54] Copyright 2017, Wiley-VCH. d) Schematic of the fabrication of rolling-up Cr/VO₂ bilayer. e) Responsive properties of the nanomembrane with external electronic stimuli. (d,e) Reproduced with permission.^[148] Copyright 2018, American Chemical Society.

3.1.2. Compound Materials on Insulator (XOI)-Based Systems

XOI system typically consists of an inorganic nanomembrane on a SiO_2 insulating layer on a semiconductor substrate. Compared with the bulk counterpart, XOI system exhibits less parasitic capacitance and lower power consumption, which makes it an excellent platform for high-performance electronic devices.^[143,144] The compound nanomembranes can be semiconductors such as silicon and germanium,^[112,142,145–147] or insulators such as nanocrystalline diamond^[54,59] and vanadium dioxide (VO_2).^[148] Other materials could be further deposited on the topmost nanomembranes to achieve more properties. For example, diamond-like carbon was deposited on silicon nanomembrane for optical regulations.^[112] Some examples of rolled-up XOI systems are given in Figure 8b–e. To release the nanomembrane, HF solution is generally used to remove the sacrificial buried oxide layer.

XOI system can also be integrated with the above MBE growth. For instance, GeSn/Ge microresonators have been epitaxially grown on Ge-on-insulator wafer.^[149] GeSn is another semiconductor material for photonic devices with tunable bandgap from 0 to 0.8 eV,^[150–153] and the rolled-up tubes further demonstrated pronounced resonant behavior.^[149]

3.1.3. Polymers

Polymers are usually stretchable, disposable, and biocompatible compared with inorganic materials, which makes them of high significance for physiological applications.^[154]

Jager et al.^[155] developed the first polymeric microactuator based on polypyrrole (PPy), polyaniline, and polythiophenes, in which the bilayer changed volume under electrochemical oxidation and reduction. The PPy could be released either by differential adhesion or sacrificial layer method, both sketched in Figure 9. In differential adhesion method, PPy was electrochemically deposited on Au layer, which was partly adhered with Cr layer. Since the major Au cannot adhere with the substrate, the bilayer rolled up upon activation. This simple method can quickly release the polymer, but it cannot apply to individually controlled microactuators. For more complex devices, a supportive metallic sacrificial layer is required.^[155] Similarly, in the work of Kalaitzidou et al.,^[156,157] thermoresponsive polymer microtubes based on PDMS and gold were developed, in which rolling-unrolling behavior was observed at 60–70 °C.

Luchnikov et al.^[49] reported another approach of rolling polymer films. In their work, PS and P4VP bilayer polymers self-rolled due to selective swelling of the bottom P4VP layer in selective solvents, as described in Section 2.1.3. This bilayer can

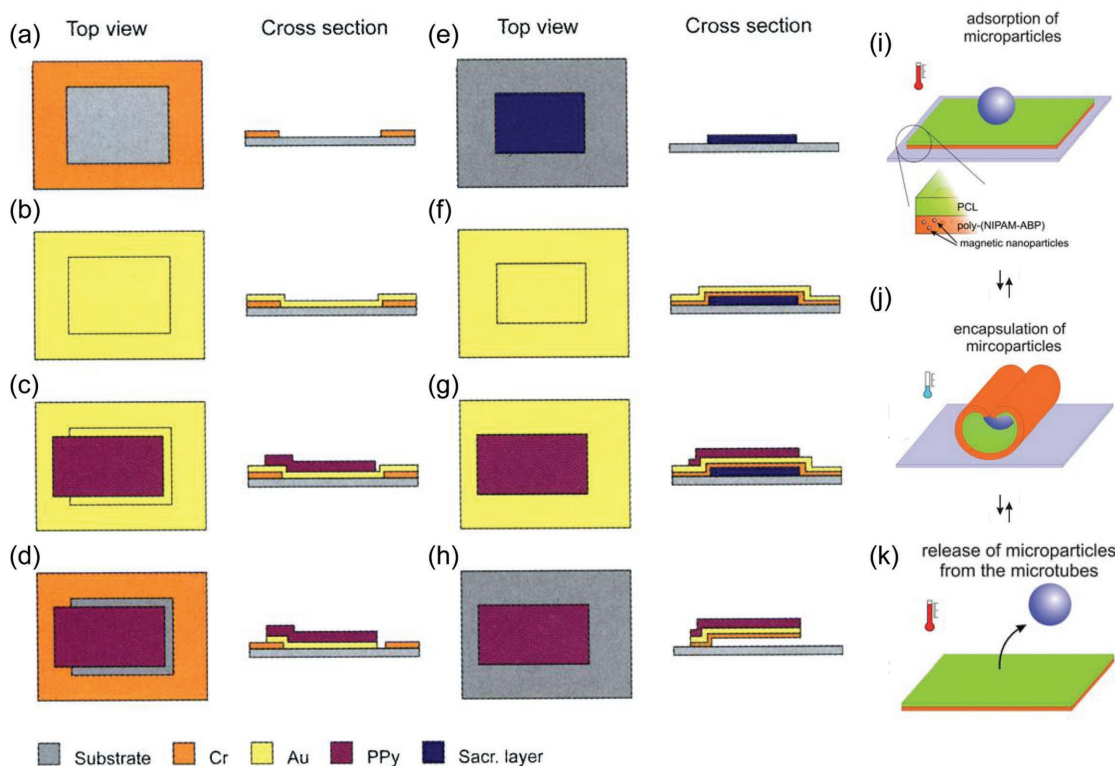


Figure 9. a–d) Schematic diagram showing the fabrication schemes for the differential adhesion method. a) Deposition and patterning of the ≈ 5 nm Cr adhesion layer. b) Deposition of the structural Au layer (≈ 100 nm). c) Electrodeposition and patterning of the PPy layer (≈ 1 μm). d) Etching of the final microactuator structure by removal of the excess Au. e–h) Schematic diagram showing the fabrication schemes for the sacrificial layer method. e) Deposition and patterning of the sacrificial layer (≈ 50 nm). f) Deposition of the Cr adhesion (≈ 5 nm) and structural Au layer (≈ 100 nm). g) Electrodeposition and patterning of the PPy layer (≈ 1 μm). h) Etching of the final microactuator structure and underetching of the sacrificial layer. (a–h) Reproduced with permission.^[155] Copyright 2000, AAAS. i–k) Schematic diagram showing the rolling and unrolling of polymer nanomembranes by cooling and heating. Adapted with permission.^[159] Copyright 2010, The Royal Society of Chemistry.

be released in acidic aqueous solutions with or without sacrificial layers. This bilayer polymer could be further applied as a template of fabricating metallic tubes and composite polymer/metal tubes can be formed utilizing swelling strain as well.^[158]

Later on, Zakharchenko et al.^[159] combined thermal response with swelling strain by utilizing thermal-swelling properties, in other words, the change in solubility of polymers at the low critical solution temperature (LCST), as shown in Figure 9i–k. The bilayer system includes a layer of polycaprolactone (PCL) and a layer of poly(N-isopropylacrylamide) copolymer containing 4-acryloylbenzophenone comonomer (poly(NIPAM-ABP)). PCL is hydrophobic and water-insoluble, while the latter material is thermoresponsive and reversibly changes its solubility in aqueous media at LCST (28 °C). Thus, when lowering the temperature from 33 to 25 °C, the bilayer starts to roll at a high speed, and microtubes are formed within 3 s. Additionally, such microtubes are able to unroll almost completely at elevated temperatures when the poly(NIPAM-ABP) is collapsed. Such combined method exhibits a reversible rolling process, greatly enhancing the versatility and broadening the application of rolled-up nanotechnology. More recently, this method was further developed for cell encapsulation by replacing the components with biocompatible and biodegradable polysuccinimide/polycaprolactone bilayers.^[160] The polymer nanomembranes can undergo different treatments of surface functionalization, making it an excellent candidate for biomedical engineering.^[160,161]

3.1.4. Rolled-up Nanotechnology on Polymers

The selective etching process in conventional fabrication typically uses caustic solutions, which not only dissolves the sacrificial layer, but also tends to damage the desired nanomembrane, and thus the requirement of high etching selectivity hindered the selection of materials choice.

To overcome this obstacle, Mei et al.^[51] developed a general rolled-up nanotechnology by depositing nonepitaxial strained

materials on polymers. **Figure 10** gives the schematic fabrication process and exemplarily shows some typical rolled-up nanomembranes using this technique. This approach has become a versatile method to fabricate micro/nanotubes out of all kinds of inorganic materials, including metals,^[162,163] insulators,^[51] and their combinations,^[164,51] on almost any flat substrates.^[113] As a result, a number of applications have been realized, including metal jet engines,^[165] optical resonators,^[51] fluidic sensors,^[58] and gas detectors.^[53] In this case, a photoresist layer is first patterned by photolithography. Strain-engineered materials are then deposited via physical or chemical vapor deposition. Acetone or other organic solvents dissolves the sacrificial photoresist without corrosion of inorganic materials, and the prestressed nanomembrane rolls up into a tubular structure.

Unlike expensive epitaxial layers, nanomembrane via non-epitaxial vapor deposition are economical in a large scale, but its polycrystalline or amorphous nature inevitably impedes its properties. In addition, the strain in nonepitaxial nanomembranes cannot be accurately identified due to extreme complexity, nor is it possible to separate one mechanism from the other.^[51] Despite such drawback, this method still remains the most commonly used way in rolled-up nanotechnology due to its superior strengths. Apart from low cost, the advantage of introducing strain in nonepitaxial grown nanomembranes lies in its versatility and the convenience to manipulate the strain value by changing deposition parameters.^[41,51]

3.1.5. 2D Materials

Since the discovery of graphene, 2D materials have sparked intense research interest due to its extraordinary characteristics. Theoretical research has predicted that rolling 2D materials can yield exceptional electronic and photonic properties.^[166–173] However, owing to the weak mechanical strength and high chemical reactivity, rolled-up 2D materials were limited to

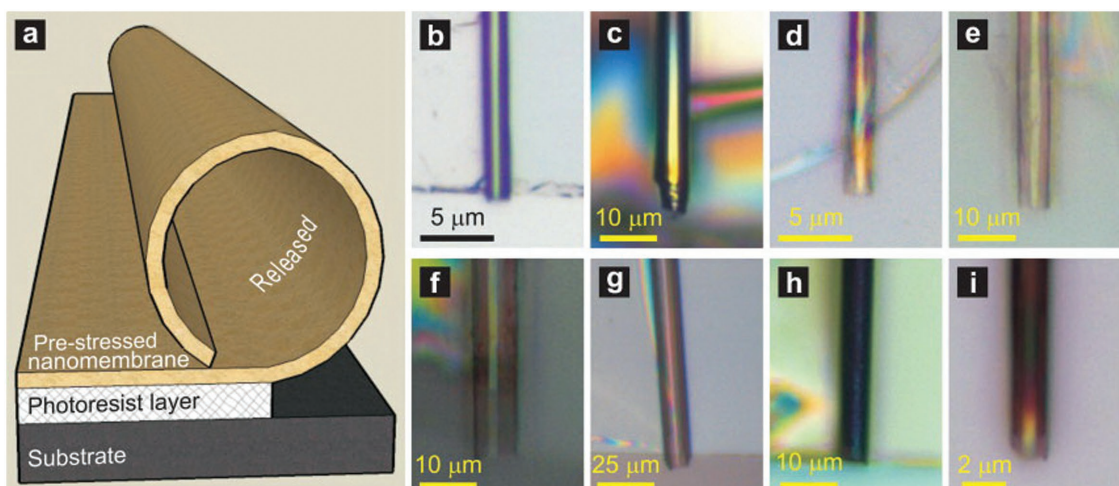


Figure 10. a) Schematic diagram illustrating the rolling process of a strain-engineered nanomembrane on a sacrificial polymer. b–i) Optical images of rolled-up nanomembranes made out of Pt, Pd/Fe/Pd, TiO₂, ZnO, Al₂O₃, Si_xN_y, Si_xN_y/Ag, and diamond-like carbon. Reproduced with permission.^[51] Copyright 2008, Wiley-VCH.

multilayer carbon,^[174–177] graphene oxide,^[111,178–181] and boron nitride (Figure 11a).^[182] These nanoscrolls were formed either by internal stress such as synthesis conditions,^[104,107,183] or external stress such as van der Waals force^[111,178,184] and magnetic field.^[185]

To resolve this limitation, researchers transferred monolayer graphene on strain-engineered epitaxial layers, as displayed in Figure 11b.^[186,187] The strained heteroepitaxial layers not only provided sufficient internal strain, but also enhanced the strength of the materials system. Therefore, the graphene sheet adhered to the wall of heterostructures during selective etching, producing tubes with well-defined diameters.

Recent advances in the synthesis of 2D materials have enabled experimental realization of rolling high-quality monolayer 2D materials alone. Utilizing surface tension of solution, Xie et al.^[97] developed a simple method to effectively roll monolayer graphene containing few impurities, as exhibited in Figure 11c. With isopropyl alcohol solution treatment, mechanical exfoliated graphene on SiO₂ substrates turned to a nanoscroll. Later on, Patra et al.^[188] predicted that water nanodroplets could also guide the folding and rolling of planar graphene sheets, where the scrolling results from the interaction between capillarity and elasticity,^[98] and this prediction was then experimentally confirmed.^[189] More recently, Cui et al.^[190] reported the rolling of transition metal dichalcogenides (TMDs) with the assistance of aqueous solutions such as ethanol. The fabricated nanoscrolls demonstrated obvious photoluminescence and stability in different atmospheres. The nanoscrolls could also hybridize with additional functional materials. Furthermore, by integrating 2D materials with thermoresponsive layers, complex 3D self-folded mesostructures could be formed with reversible deformation.^[191,192]

3.1.6. Other Materials Systems

There are some other materials systems that could release the nanomembranes by wet etching the sacrificial layers. For instance, a metal nanomembrane can be obtained by etching aluminum in KOH-based etchant,^[193] and undoped GaN could be released by electrochemical etching of heavily doped n-type GaN in a HF-based solution.^[194] In fact, rolled-up nanotechnology can be applied to many other materials systems as long as there exists an etching selectivity between the desired materials and sacrificial ones.

3.2. Dry Release

Apart from wet etching, dry-etching sacrificial layer can also be applied to release nanomembranes. For instance, Al_xGa_{1-x}As can be released with gaseous XeF₂ etchant by removing the sacrificial Ge layer.^[195] Similarly, suspended nanomechanical devices can be fabricated using HF vapor to etch away the SiO₂ sacrificial layer.^[196] However, such fabrication process inevitably introduces dangerous gaseous etchant, which is demanding to the equipment and harmful to the environment.

Recently, an alternative dry-release method was developed in which burning of sacrificial layers replaced traditional etching process.^[52] As mentioned in Section 2.2.1, with RTA treatment, the decomposition of PMMA sacrificial layer led to the release of nanomembranes. Furthermore, in this process the produced metal nanodroplets provided enhanced surface area, resulting in higher moving velocities of the micro/nanomotors.^[52] Compared with etching sacrificial layer, which requires critical point drying (CPD) subsequently to prevent structural collapse due

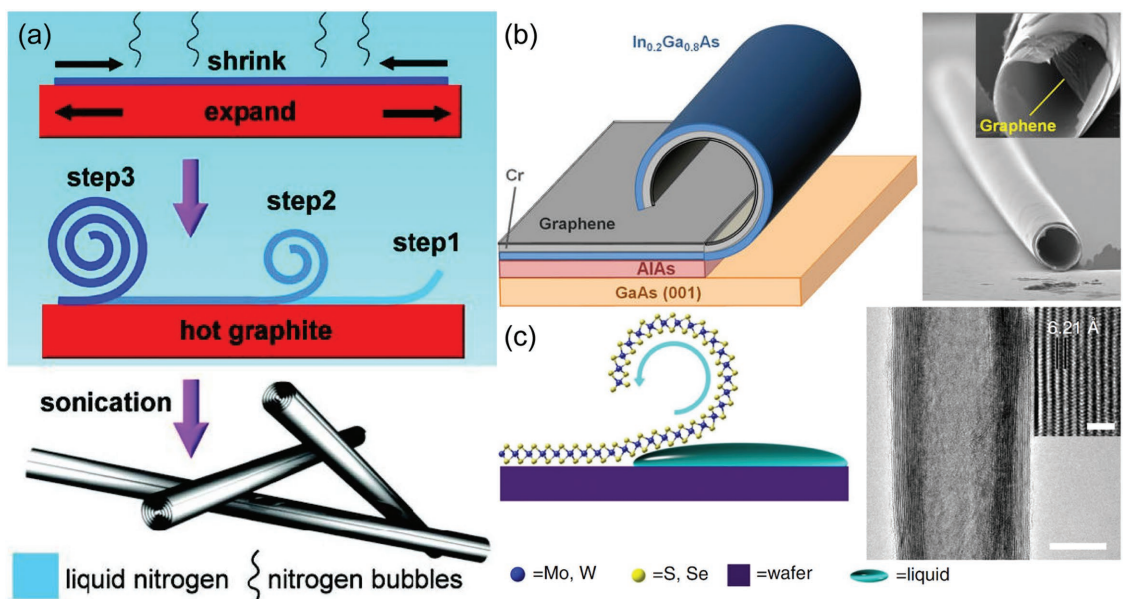


Figure 11. a) Schematic illustration of the fabrication process of a carbon nanoscroll. The graphite flakes were rapidly heated by microwave irradiation and then cooled by liquid nitrogen. Reproduced with permission.^[174] Copyright 2011, Wiley-VCH. b) Production of rolled-up tubes of InGaAs/Cr/graphene and SEM images of the tube. Adapted with permission.^[186] Copyright 2014, American Chemical Society. c) Schematic of rolling TMD monolayer flakes and TEM images of MoS₂ nanoscrolls (scale bars: 20 nm; inset = 2 nm). Adapted with permission.^[190] Copyright 2018, Springer Nature.

to the surface tension at the liquid interface and tends to bring damages to the fabricated fine structures, the dry releasing approach offers an economical and simple opportunity for releasing nanomembranes.

3.3. Ultrasonication Treatment

As mentioned in Section 2, ultrasonication treatment can act as an external force to induce the rolling of some nanomembranes system. When the bonding between the nanomembranes and the substrate is not strong, ultrasonication treatment can also serve to destroy such bonding, inducing the detaching between the two and eventually triggering the rolling-up process. To create an easily detachable interface between nanomembranes and the substrate, tissue cells extracted from fruits of banana and apple are applied.^[197] As shown in Figure 12a, banana cells were first uniformly deposited on a glass cover slip. After the complete evaporation of water, Pt was deposited on the cells-coated glass coverslip by sputtering. Upon the sonication of the nanomembranes system in water, tissue cells detached from the glass cover slip, leading to the instantaneous formation of cells/Pt microtubes (Figure 12b). Such detaching method eliminates the etching process using chemical solutions and effectively shortens the total fabrication time.

Additionally, nanomembranes could be released from the substrate via ultrasonication treatment even without the assistance of an interface layer such as the tissue cells mentioned above. As shown in Figure 12c,^[163] a glass coverslip was first treated in oxygen plasma to create a hydrophilic surface and then a TEM grid was directly placed on it. After the deposition of Pt via sputtering and removing TEM grid, the nanomembranes system was exposed to H₂O₂ solution with ultrasonication treatment. The sound energy together with the bubble evolution

generated at the edges of the Pt films eventually led to the detaching of Pt with the glass substrate and the formation of microtubes (Figure 12d).

Furthermore, it should also be noted that the above mentioned two strategies are both clean-room-free methods which do not require photolithography process, effectively reducing the cost for the fabrication of microtubes via rolled-up nanotechnology.

4. Discussion

In this section, we will review the tenability of rolled-up nanotechnology. The morphological properties of 3D nanostructures fabricated via rolled-up nanotechnology will be discussed in details, including the formation of wrinkles or microtubes, the curvature of rolled-up nanostructures, the rolling direction of nanomembranes, and the change of chirality in helical structures.

4.1. Wrinkling or Bending?

When subjected to compressive strain, a membrane system can relax via either wrinkling or bending.^[33,48] Generally, when the strain gradient across the membrane is large, the membrane tends to bend into microtubes, while small or zero strain gradient leads to the wrinkling of the membrane.^[198] Such phenomenon could also be explained in the aspect of energy, as the final morphology of the 3D nanostructure exhibits the minimal total energy.

The investigation of bilayer system with isotropically elastic properties has shown that the wrinkling or bending behavior of nanomembranes could be quantitatively determined.^[198] Isotropic materials exhibit the same Young's modulus along

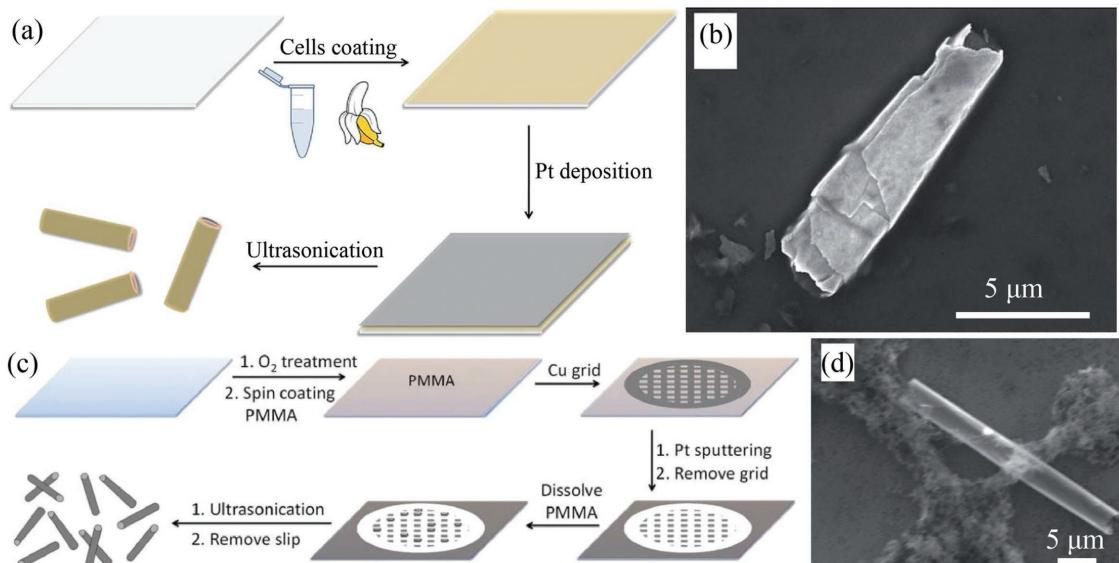


Figure 12. a) Illustration of fabrication process of Pt microtubes with the aid of tissue cells. The ultrasonication serves to detach the Pt nanomembranes from the substrate. b) SEM image of cells/Pt microtubes. (a,b) Adapted and reproduced with permission.^[197] Copyright 2014, The Royal Society of Chemistry. c) Schematic diagram showing the rolling of Pt microtubes with ultrasonication-assisted detaching process. d) SEM image of Pt microtubes. (c,d) Reproduced with permission.^[163] Copyright 2014, The Royal Society of Chemistry.

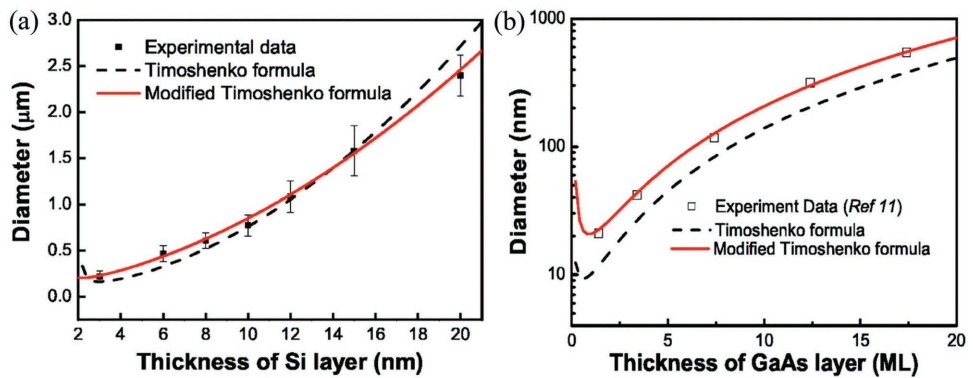


Figure 13. Schematic diagram of a) partially relaxed free-hanging bilayer nanomembranes system, b) the bending and c) wrinkling of nanomembranes upon strain relaxation. d) The wrinkle energy and e) the wrinkle wavelength and amplitude as a function of the etching length h . f) Phase diagram of the energetically favorable morphology of relaxed prestrained nanomembranes. Solid curve shows the boundary between bent and wrinkled shapes. R_{eq} is shown for the bent structure and wavelength λ for the wrinkled structure. Dashed curve shows the phase boundary curve for $\bar{\epsilon} = -1.0\%$. Adapted with permission.^[198] Copyright 2009, American Physical Society.

all directions,^[17,41] and thus there is no specific energetically favorable direction to bend if no boundary constraint exists. Consider two isotropic nanomembranes with thickness d_1 and d_2 , which are subjected to biaxial strain ε_1 and ε_2 , respectively. As shown in Figure 13, the nanomembranes are partially relaxed with a free hanging portion which could relax elastically and is only constrained by the fixed boundary,^[198] marked by dashed lines in Figure 13a. The total length of the nanomembranes is defined as L , while h is the etching length satisfying $L \gg h$. The strain gradient and average strain of the nanomembranes system are defined as $\Delta\varepsilon = \varepsilon_2 - \varepsilon_1$ and $\bar{\epsilon} = (\varepsilon_1 d_1 + \varepsilon_2 d_2)/(d_1 + d_2)$, respectively. For small h , the relaxation along x direction is limited by the confinement of boundary conditions, and thus only relaxation along y direction will occur, leading to the bending of nanomembranes, as shown in Figure 13b. As h increases, the confinement from fixed boundary becomes weaker, making the relaxation along x direction more energetically favorable and thus leading to the formation of wrinkles, as displayed in Figure 13c. Obviously, the etching length must exceed a certain critical value h_{cw} for the formation of wrinkles.^[198] According to theoretical calculation, h_{cw} was found to be $h_{cw} \approx 2.57d_2\sqrt{-\bar{\epsilon}}$. The wrinkle energy was also calculated and is shown in Figure 13d. When $h < h_{cw}$ the nanomembranes would only planarly relax along y direction and thus only bending would occur. When $h < h_{cw}$ wrinkling can occur with energy lower than the planer value. Besides, as shown in Figure 13e, the amplitude and wavelength of wrinkles would also increase as h increase. However, large h value ($h > h_{cw}$) does not necessarily lead to the formation of wrinkles. Experiments have shown that large strain gradient might induce the bending of nanomembranes even $h > h_{cw}$ is satisfied.^[17,41]

Actually, as mentioned above, the final morphology of 3D structures can be determined by the total energy of the system, which depends on strain gradient, etching length, and nanomembranes thickness. The investigation of the wrinkling or bending nanomembranes system has been reported.^[198] Considering a bilayer system consisting of 10 nm In_{0.1}Ga_{0.9}As and 10 nm GaAs. The Young's modulus Y and Poisson's ratio ν of the two layers were set to be equal ($Y = 80$ GPa and $\nu = 0.31$),

and the value of ε_1 and ε_2 were changed to calculate the most energetically favorable morphology. The calculated favorable shape as a function of h and strain gradient is shown in the phase diagram in Figure 13f. The boundary between wrinkling and rolling was clearly marked by a solid line. According to this line, the critical h_{cw} value under certain strain status could be identified. For example, when $\Delta\varepsilon = 0.20\%$ and $\bar{\epsilon} = -0.36\%$, bending would dominate only when $h < h_{cw} \approx 700$ nm. For larger h , the wrinkled morphology would exhibit a lower total energy than bending structure and thus becomes energetically favorable. When considering higher average strain, that is, $\bar{\epsilon} = -1.0\%$ (dashed line in Figure 13f), the phase boundary would move upward while the wrinkling region would be larger.

When the elastic properties of the nanomembranes system are anisotropic, the situation would be different.^[17,41] Anisotropic materials exhibit direction-dependent Young's modulus, and the direction with the smallest Young's modulus exhibits the minimum bending energy. Such direction is the easiest to bend, and thus is the most compliant direction. For example, the most compliant direction of single-crystal Si is $\langle 100 \rangle$.^[199,200] Therefore, it is energetically favorable for prestrained anisotropic Si nanomembranes to bend along $\langle 100 \rangle$. Considering the same coordinate system as in Figure 13 for anisotropic nanomembranes. If the y direction is the most compliant direction, the nanomembranes would bend or roll along y . On the contrary, when x direction is the most compliant direction, though the nanomembranes tend to bend along this direction as it is the most energetically favorable, the boundary constraints might hinder such tendency. As a compromise, wrinkles would be formed to relax strain. Similar to the isotropic situation, there exists a crucial etching length h_{cw} for the formation of wrinkles. At the beginning of the etching when $h < h_{cw}$, the boundary constraint is so close to the free ending that the strain remains in the nanomembranes without any wrinkling or bending. Once $h > h_{cw}$ wrinkles would form. Such phenomenon has been demonstrated in experiments, where the wavelength of wrinkles decreases while the amplitude increases with increasing h , because the nanomembranes tend to form narrow and high wrinkles as it prefers to relax along x direction.^[201]

4.2. The Curvature of Rolled Nanostructures

As mentioned above, the prestrained nanomembranes system bends or wrinkles as a result of strain relaxation, and the final morphology exhibits the lowest total energy. Thus, for a certain nanomembranes system, the bending curvature of the rolled nanostructures (or the diameter of the microtubes) could be determined by its strain gradient and nanomembrane thickness.^[51,135] Consider a prestrained bilayer system with the thicknesses of d_1 and d_2 , and the Young's moduli of Y_1 and Y_2 , respectively. Utilizing a continuum mechanical model (Timoshenko model), the bending curvature of the rolled-up nanostructures could be expressed as^[135,201–204]

$$\kappa = \frac{6\epsilon(1+m)^2}{d[3(1+m)^2 + (1+m\cdot n)\cdot[m^2 + (m\cdot n)^{-1}]]} \quad (1)$$

where $d = d_1 + d_2$ is the total thickness of the bilayer, ϵ is the in-plane biaxial strain between the two layers, $n = Y_1/Y_2$ and $m = d_1/d_2$ are the ratio of Young's modulus and the thicknesses of the top and bottom layer, respectively. For a single prestrained nanomembrane, the curvature of the rolled nanostructures could also be calculated by utilizing the bilayer model, which assumes that the nanomembrane consists of two layers with equal thicknesses. In this way, m and n are both assumed to be 1, and Equation (1) could be simplified as $\kappa = -3\epsilon/(2d)$.

Equation (1) is also referred to as the Timoshenko formula as it was established by Timoshenko over a century ago to describe the bending performance of macroscopic films.^[204] Though it also serves well for nanomembranes with relatively large thickness, the results calculated from Timoshenko formula derived from experimental results for ultrathin nanomembranes with only a few monolayers.^[205] Such discrepancy could be attributed to the surface stress which becomes more dominant due to surface reconstruction or chemical modification in ultrathin nanomembranes. The bending of nanomembranes with only a few monolayers is a combined result of intrinsic strain gradient and the surface stress. Thus Timoshenko formula, which only considers the intrinsic strain gradient, exhibits increasing deviation from the experiments with decreasing thickness. A modified Timoshenko formula was later proposed to take the surface stress of ultrathin nanomembranes into consideration. The detailed deviation could be found in ref. [205]. The diameters of microtubes predicted by the modified Timoshenko formula exhibited decent agreement with the experimental

results, as shown in Figure 14. In details, Figure 14a shows the variation of pure Si microtubes diameters with varying Si thickness.^[124,205] The black dots are experimental results, which obviously exhibits slight discrepancy with the classical continuum model (dashed line) but shows good fit with the modified

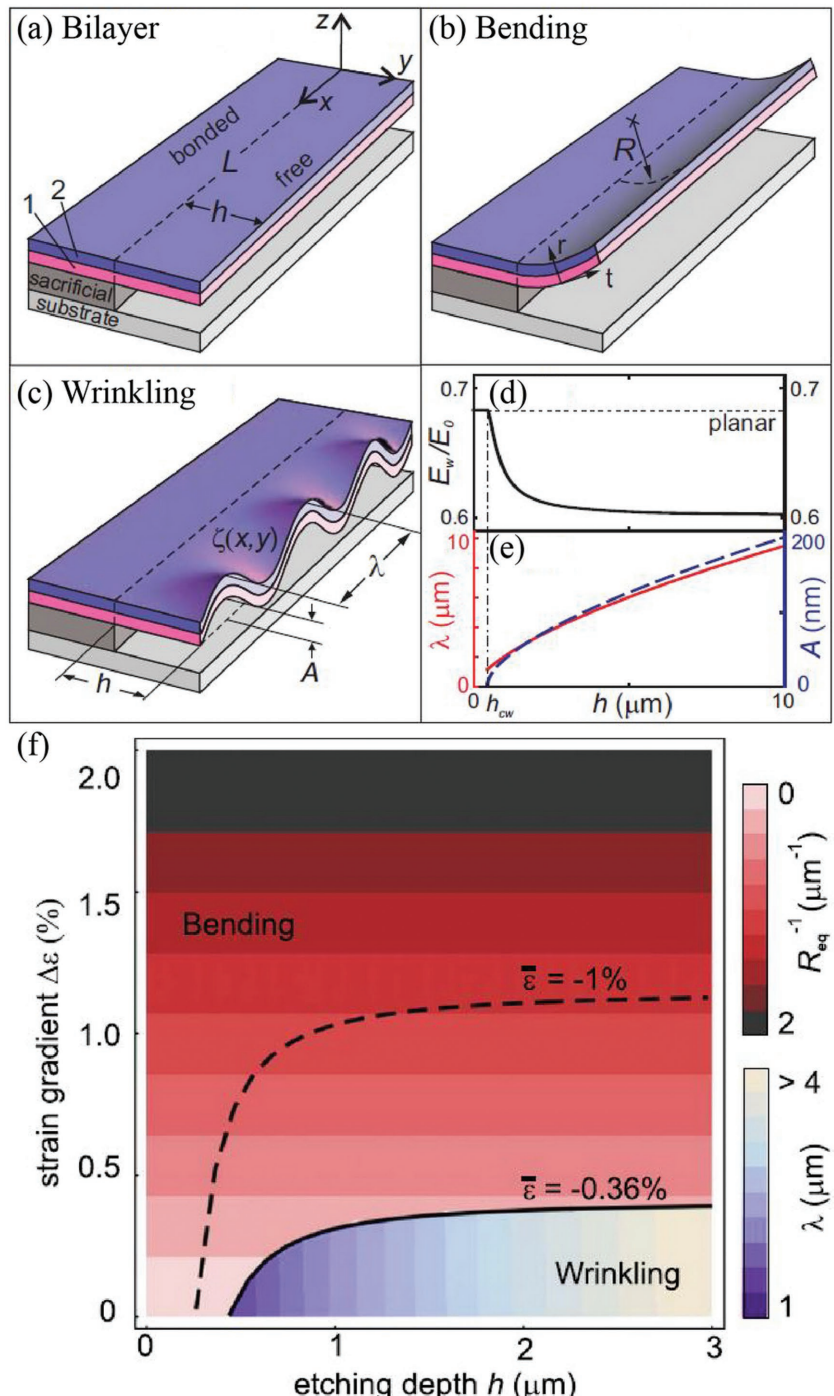


Figure 14. a) Diameters of single-layer Si microtubes as a function of thickness. The thickness of strained Si layer is fixed at 2 nm. b) Diameters of InAs/GaAs microtubes as a function of GaAs layer. The thickness of InAs layer is fixed at two monolayers. Adapted with permission.^[205] Copyright 2008, American Institute of Physics.

Timoshenko formula. Such phenomenon could also be observed in Figure 14b, which plots the diameters of InAs/GaAs microtubes as a function of GaAs thickness while the thickness of InAs is fixed at bilayer.^[135,205]

4.3. Rolling Direction

For patterned nanomembranes system, the rolling direction upon releasing is a significant factor determining the final morphology of the rolled nanostructures. As has been briefly discussed earlier, the nanomembranes with anisotropic properties would roll along the most compliant direction. However, the situation of isotropic nanomembranes system is more complicated. As mentioned above, isotropic materials exhibit no specific energetically favorable rolling direction and tend to roll with an optimal radius regardless of direction. However, for pattern nanomembranes such as strips (with width W and length L), the situation is different.^[42,206] If the curvature of the nanostructures calculated from Timoshenko formula is κ , then the inner perimeter length of the microtubes which complete one circle is $L_0 = 2\pi/\kappa$. When $L > L_0$, if the nanomembranes still roll along the same direction parallel to L , then extra rotation would induce more rotations, resulting in the increase of rolling radius. Such increase would bring extra elastic energy to the whole system, making such morphology energetically unfavorable. Thus, under such circumstance, the nanomembranes strip would form helical structure instead of microtubes with a rolling direction which exhibits an angle θ to the long side of the strip. Such rolling behavior would reduce the total energy of the system by allowing each rotation in the helical structure to adopt the optimal radius, despite the fact that extra shear energy is introduced. However, only when the shear energy induced by helical structure is lower than the extra energy from larger rolling radius could helical morphology be energetically favorable. Thus, there exists a critical angle $\theta_c = \sin^{-1}(W/L_0)$ and only under the condition of $\theta > \theta_c$ would helical structures form.^[42] Otherwise, the nanomembranes would still roll into microtubes.

However, when considering etching process (such as wet etching), the patterned nanomembranes are not released from the substrate immediately but rather gradually, because the sacrificial layer starts to dissolve upon contacting with etchants. Thus, all sides of patterned nanomembranes would bend initially once they are released from the substrate and final rolling behavior is hard to control (i.e., the poor rolling behavior at the pattern corners).^[207,208] Several methods have been proposed to manipulate the rolling behavior of patterned nanomembranes and induce the nanomembranes to roll along the desired direction with accurate positioning.

The first method is shallow etching,^[207] as shown in Figure 15a. A deep mesa structure was created on the top of InGaAs/GaAs bilayer grown on a GaAs (100)-oriented substrate via MBE. Then certain part of the upper GaAs layer was removed in a second lithography step and a shallow mesastructure was obtained. Upon releasing the nanomembranes from GaAs substrate, the strain-free single InGaAs layer would not bend and only the shallow mesastructure area could roll due to strain relaxation. The adjacent InGaAs layer at the boundary was ruptured during the rolling process as a result

of mechanical stresses concentration. In this way, the patterned bilayer would roll along the desired direction without any poor rolling behavior at corners.

The other method is glancing angle deposition (GLAD) techniques,^[51] which could be used in normal physical vapor deposition methods such as electron beam or thermal evaporation as well as sputtering. As shown in Figure 15b, the sacrificial layer (photoresist) was patterned into rectangles by photolithography and strained nanomembranes were deposited onto the tilted substrate. In this case, a narrow gap remained open after deposition at the far end of the patterned sacrificial layer due to the ballistic shadow effect that always occurs in GLAD.^[209] Thus, the etchants would enter the gap and the etching process started only from this gap, leading to the formation of microtubes array with well-defined direction.

Furthermore, the rolling process and final morphology of nanomembranes with rectangular patterns are of great interest, as rectangle is a basic shape and many other complex pattern could be regarded as a combination of rectangles. The rolling behavior of rectangle nanomembranes upon isotropic etching has been investigated both experimentally and theoretically.^[210,211] Generally, nanomembranes with rectangular shapes would preferably roll along the direction perpendicular to the long side. As shown in Figure 15c, though both the long side and the short side of rectangle start to roll at the beginning due to the simultaneously and isotropic etching process, the curved short side compromises by opening itself up to allow continued rolling from the long side as the etching proceed with increasing portion of free nanomembranes. Such preferable rolling direction could be explained by the larger bending force to roll perpendicular to the long side than the bending force to roll parallel to the long side, which has been justified by the simulation with finite element method.^[210] However, short-side rolling behavior has also been observed in experiments. This is because the total energy of final morphology is not the only factor influencing the rolling direction. The deformation history, which could influence the experimental process such as etching rate in different directions, might also determine the rolling direction depending on the intermediate status. Nevertheless, long-side rolling is still dominant for rectangular-patterned nanomembranes. Moreover, anisotropic etching process kinetically created via lithographical patterning could force the rectangle nanomembranes to exhibit long-side rolling with 100% yield.^[210]

To change such long-side rolling dominance and make the rectangle nanomembranes roll along the short side, a method utilizing wrinkles has been proposed.^[208] As shown in Figure 15d, when a rectangular prestrained wrinkled nanomembrane is gradually released from its substrate, it would either roll along the wrinkled edge and form a tube at wrinkled edge (TWE) or roll along the flat edge and form a tube at flat edge (TFE). Theoretical study showed that TFE is the energetically favorable morphology as bending from the wrinkled edge would be suppressed by an energy barrier arising from the need to flatten the wrinkles. Experiments based on such wrinkled structures have also been performed, as shown in Figure 15e–h. The wrinkled rectangle nanomembranes were prepared by deposition of metallic CuNiMn alloyed nanomembranes on wrinkled surfaces of photoresist and the lithographic step afterward.

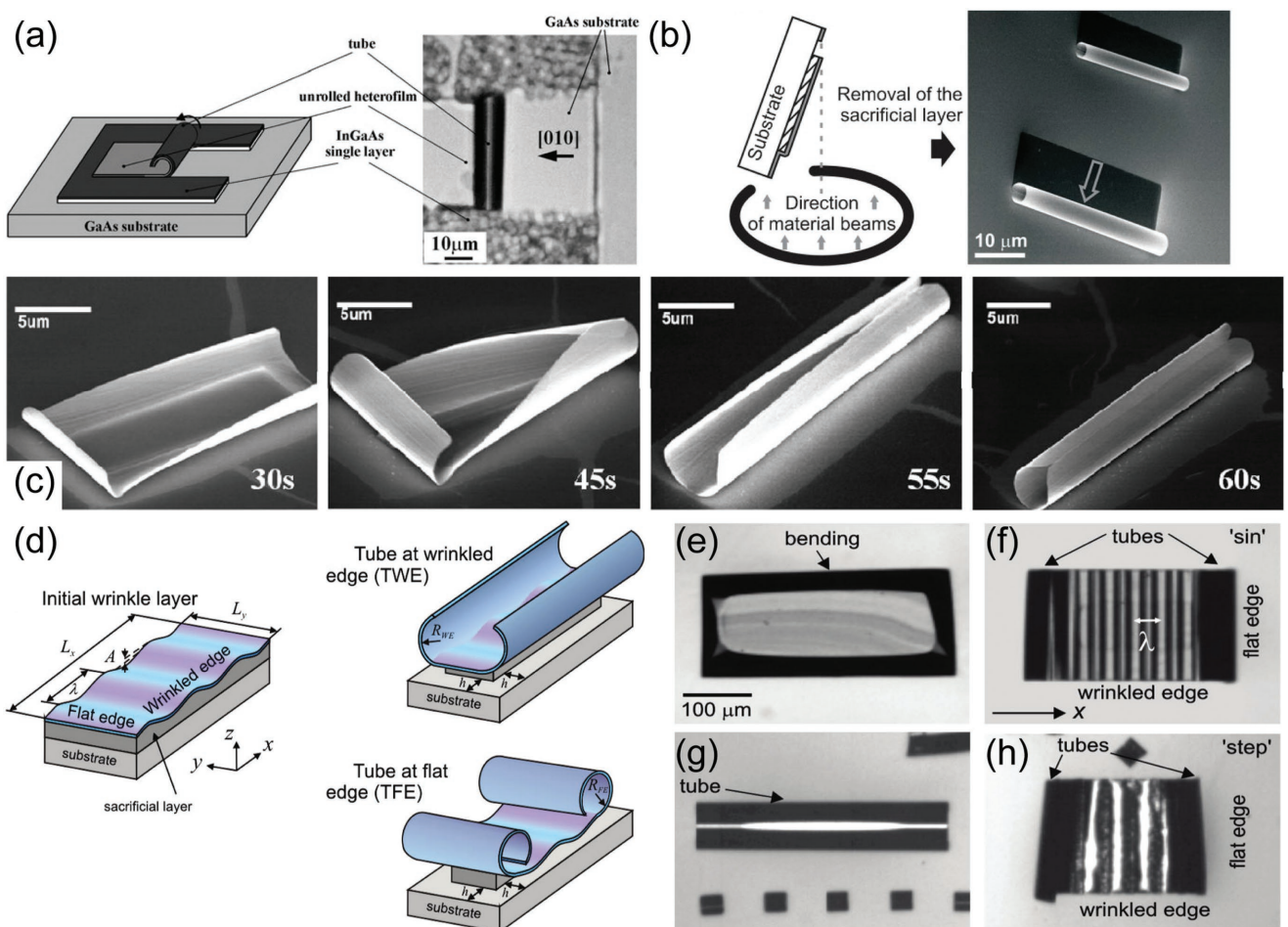


Figure 15. a) Illustration of shallow etching method to eliminate the poor rolling behavior at the corners. Reproduced with permission.^[207] Copyright 2002, IOP Publishing. b) Tilted deposition method utilizing the ballistic shadow effect and SEM image of rolled-up Ti/Au microtubes exhibiting well-defined direction. Reproduced with permission.^[51] Copyright 2008, Wiley-VCH. c) SEM images showing nanomembranes with long-side rolling behavior. Reproduced with permission.^[210] Copyright 2010, American Chemical Society. d) Schematic diagram showing the structures of initial wrinkle layer, tube at wrinkled edge, and tube at flat edge. e–h) Optical microscopy image showing the rolling process of flat and wrinkled nanomembranes. The flat nanomembrane exhibits long-side rolling behavior while the wrinkled nanomembrane rolls from the short side. (d–h) Reproduced with permission.^[208] Copyright 2018, American Chemical Society.

Upon contacting with droplets of N-methyl-2-pyrrolidone to selectively remove the sacrificial layer, the wrinkled nanomembranes would roll along the flat edge (short side) and eventually form a TFE. In comparison, flat nanomembranes would roll along the long side as discussed above. Thus, such method utilizing wrinkled structures could break the long-side rolling dominance and induce the short-side rolling of rectangle nanomembranes.^[208] Additionally, researchers recently proposed a transient quasi-static finite element method^[212] which could precisely predict the rolling behavior and final dimensions of silicon nitride nanomembranes, further improving the controllability and design accuracy of rolled-up nanotechnology.

4.4. Change of Chirality

The helical structures are chiral structures with broken left-right symmetry of which the handedness or chirality could be tuned intentionally.^[46,213]

In an anisotropic materials system, the rolling direction depends on the misaligned angle between the anisotropic driving force direction and the crystal orientation.^[46,126,214] For example, researchers can control the formation of InGaAs/GaAs nanosprings with different pitches by changing the pattern orientations (Figure 16).

Besides geometric designs, the dimensions of the structures may have an impact on the twisting direction as well. As shown in Figure 16a–h, Zhang et al.^[74] studied the rolling phenomena of SiGe/Si and SiGe/Si/Cr nanobelts. When the width of the strips decreases from 1.3 to 0.7 μm, the chirality of the helix switches from right-handed, to mixed, and to left-handed with the same misorientation angle of 10° from ⟨110⟩, which was explained by the dominance of edge effects over crystal properties.

On the other hand, in an isotropic system the uniaxial shearing force guides the twisting of the structure.^[46] For example, as displayed in Figure 16j,k, the chirality of nanocrystalline diamond helical structures could be controlled by designing asymmetric shapes.^[54,59] Through patterning

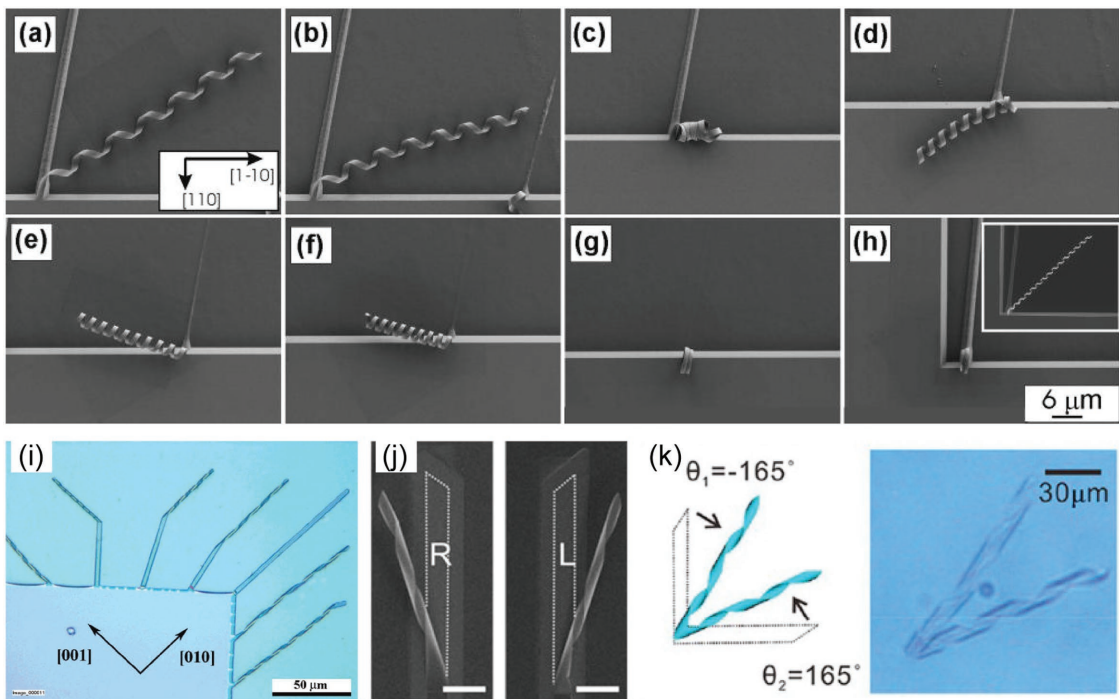


Figure 16. a–h) Helical coils with decreasing width of the stripes stepwise from 1.30 to 0.70 μm . Reproduced with permission.^[74] Copyright 2006, American Chemical Society. i) Helical structures with different initial orientations. Reproduced with permission.^[116] Copyright 2006, American Chemical Society. j) Opposite chirality fabricated by diagonal rolling (scale bars: 30 μm). k) Rolling of interconnected helices showing opposite chirality. (j,k) Adapted with permission.^[59] Copyright 2018, American Chemical Society.

strained nanomembrane into hockey stick or utility knife shape, the imbalance of etching rates along different sides generated anisotropic mechanical stress, making the nanomembrane roll into a helical structure, which agreed well with the finite element method model. Furthermore, helical framework was fabricated based on this model that reversed its chirality midway mimicking the shape of natural plant tendrils.

The chirality of helical structures can be further modified on the basis of materials properties. For instance, Erb et al.^[215] developed self-shaping composites with orientational control by combining the reinforcement of inorganic particles with swellable/shrinkable polymer matrices. Later on, in the work of de Haan et al.,^[216] liquid crystal polymer network changed its chirality when stimulated by humidity. One side of the polymer sheet is treated with KOH or rinsed with water. When the ribbon is wet, the sheet bends toward the untreated side; when dried, it bends toward the other side. By misaligning the ribbon to the swelling and shrinking direction, humidity-sensitive curling actuators were prepared in which wet and dry states demonstrated reversed handedness.

5. Rolling or Bending for Mesostructures

Apart from micro- and nanotubes, other nanostructures could also be demonstrated utilizing rolling or bending process. Such 3D complex structures, or mesostructures,^[31,45] exhibit decent properties that could not be observed in natural world and offer great application potentials in various fields. In this section,

mesostructures fabricated via strain engineering are discussed and summarized.

5.1. Rolling with Particular 2D Patterns

The most straightforward method to fabricate 3D structures with complex morphologies based on rolled-up nanotechnology is to roll nanomembranes with particular 2D patterns. Microtubes are usually demonstrated with rectangular-shaped nanomembranes,^[51,210] while U-shape patterns^[120,217,218] are also commonly used to fabricate freestanding tubular optical microcavities. Additionally, not only the nanomembranes with patterns at the edge but also throughout the entire nanomembranes have been studied, resulting in microtubes with patterns on the tube wall.^[121] Furthermore, more complicated 3D structures such as 3D jagged ribbon, ring-in-ring, tube-in-tube, and helix could also be demonstrated utilizing carefully designed 2D patterns,^[54] as shown in Figure 1f. Additionally, the manipulation of rolling direction and curvatures of the rolled-up nanostructures mentioned before should also be taken into consideration for the design of 2D patterns to fabricate 3D complex structures.^[219] More mesostructures presented in this way are shown in Figure 17.^[74,219–222]

5.2. Bending at the Hinges

Nanomembranes with built-in strain could be incorporated into self-folded systems to fabricate polyhedra, which could

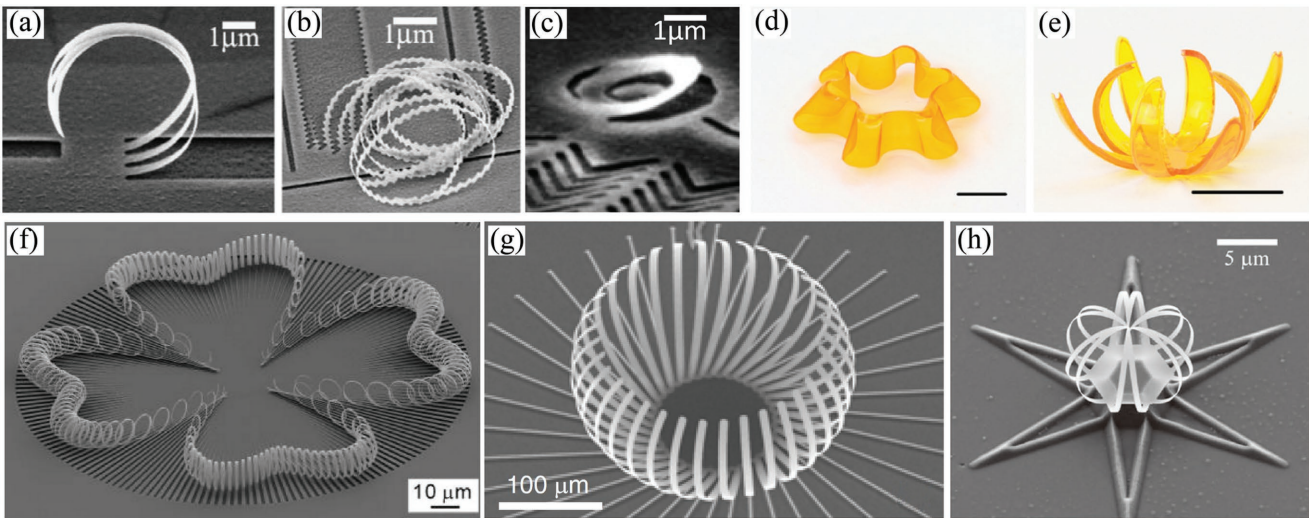


Figure 17. Mesostructures fabricated via rolling and bending nanomembranes with particular patterns. a) Bent cantile, b) nanosaw, and c) archimedean spiral-like strip rolled from SiGe/Si bilayer system with a total thickness of 35 nm. (a–c) Adapted with permission.^[222] Copyright 2001, IOP Publishing. d) Wavy ring and e) flower (scale bars: 10 mm) made from a bilayer of hydrophilic rubber poly(ethylene glycol) diacrylate and hydrophobic rubber poly(propylene glycol)dimethacrylate. (d,e) Adapted with permission.^[221] Copyright 2018, American Chemical Society. f) Ringlike structure formed from a bilayer of p-type crystalline Si and amorphous Cr. Reproduced with permission.^[74] Copyright 2006, American Chemical Society. g) Released tilted structure rolled from 50-60-50 nm Cr-Ni-Cr films. Adapted with permission.^[219] Copyright 2007, IOP Publishing. h) Metallic flower cage made from a Ti (5 nm)/Al (25 nm)/Cr (20 nm) film. Reproduced with permission.^[220] Copyright 2013, Wiley-VCH.

serve as containers. Although the self-assembly of lithographically structured polyhedra has been reported utilizing the surface tension of electrodeposited either on top or in between of individual rigid segments,^[35,223–225] such method could not be used at room temperature given the high melting point of the solder. However, bending could be used at the flexible hinges to demonstrate polyhedra at room temperature.^[226–228] As shown in Figure 18a-i, the low-temperature self-assembly of polyhedra is enabled with a trilayer of Cr/Cu/polymer hinges^[226,229] connecting lithographically patterned faces arranged as a cruciform. The polymer demonstrates high flexibility when heated, but is stiff under room temperature, serving to prevent spontaneously folding once released. The folding of 2D cruciform and the self-assembly of polyhedra upon releasing and heating is enabled by the bending of bimetallic component of Cr and Cu. The built-in strain of the bilayer mainly comes from the intrinsic tension in Cr during growth, and is partially due to the mismatch in the thermal expansion coefficient of Cu and Cr.^[230] It should be noted that both upward and downward folding are possible with the Cr layer above or below the Cu layer, and the angle of folding could be controlled by the thickness of Cr. The polyhedra prepared by this method are shown in Figure 18a-ii–iv.

Utilizing the mechanism above, more complicated 3D structures have been prepared. As shown in Figure 18b-i,ii,^[231] the 2D cruciform is extended into a network consisting of three distinct areas: rigid segments, flexible hinges, and hollow regions. Rigid segments are designed to prevent local deformation of the sheet, containing thick Ni segments on top of the Cr/Cu bilayer, while at flexible hinges the polymer segments take the place of Ni. When the sacrificial layer is dissolved in water, the sheets lift off from the substrate and gradually assemble into complex 3D structures.^[231] The final morphology of the mesostructures after assembly depends on the 2D lithographical

patterns, or in other words, the connections of rigid segments by flexible hinges. Using different patterns of square lattice (Figure 18b-iii), different 3D structures such as spiral, woven coil, coil, diagonal cylinder, and orthogonal cylinder have been demonstrated (Figure 18b-iv). Furthermore, the curvature of mesostructures at the flexible hinges as well as the rigid segments could be well predicted and tuned by the thickness and modulus of the multilayer.^[232]

These two methods which utilize bending at the hinges, though capable of fabricating mesostructures with great complexity, are limited in one aspect: these structures could fold in only one direction. By further manipulating the strategy, researchers have achieved spontaneous bidirectional folds with any desired angles, and complex 3D structures with +90°, -90°, +180°, -180° folds have been both theoretically demonstrated and experimentally realized.^[233] As shown in Figure 18c-i, by depositing an additional prestrained layer of Cr in designed positions, two kinds of hinges are obtained:^[234] (1) Cr/Cu bilayer hinges which bend into the substrate, and (2) trilayer hinges of Cr/Cu/Cr which bend away from the substrate. In this way, bidirectional folding occurs as a result of large residual tensile strain within the Cr layer, while the Cu layer provides structural support.^[235] The folding angle could be manipulated by changing the thickness of Cr and the final morphology also depends on the ratio of rigid panel lengths and hinge length. Examples of the mesostructures (cubic core structures)^[236,237] fabricated by this method could be seen in Figure 18c-ii,iii.^[233]

5.3. Rolling/Bending in 4D Structures

The evolution of morphology according to the change in environment or external stimulation might result in more

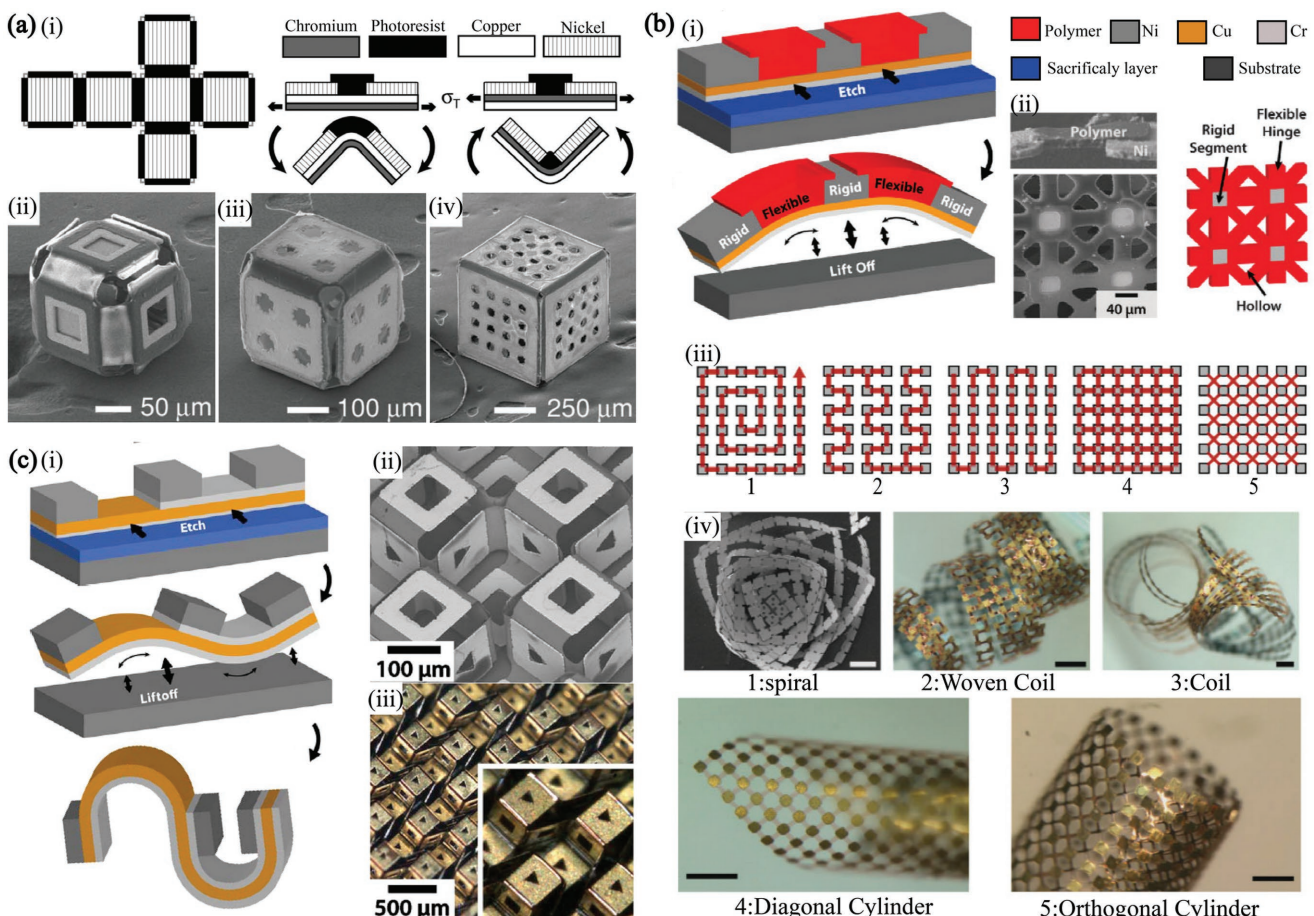


Figure 18. The mechanisms and fabrication of mesostructures utilizing bending at the hinges. a) Demonstration of a single microcube with prestrained bilayer as the flexible hinges. (i) Schematic diagram showing the 2D cruciform and trilayer hinges. (ii-iv) Differently sized polyhedra with varied surface composition and porosity. (ii,iii) are 100 and 200 μm in size, formed by downward folding, while (iv) is 500 μm in size, formed by upward folding. Adapted with permission.^[226] Copyright 2008, Wiley-VCH. b) Design concept and assembly process of 3D complex structures based on 2D sheets with lithographically patterned mechanical properties. (i) Schematic diagram showing the etching and the afterward lifting off process of 2D sheets. (ii) SEM image of the side view (left top) and top view (left bottom) of the sheets, and illustration (right) showing the rigid segments, flexible segment, and hollow regions. (iii) Different 2D sheets patterns and the corresponding formation of (iv) different mesostructures. 1: spiral; 2: woven coil; 3: coil; 4: diagonal cylinder, and 5: orthogonal cylinder (scale bars: 250 μm). Adapted with permission.^[231] Copyright 2008, Wiley-VCH. c) Spontaneous bidirectional folding. (i) Schematic diagram showing the design concept of 2D precursors. (ii,iii) 3D complex structures fabricated utilizing spontaneous bidirectional folding, with square pores on horizontal faces and triangular pores on vertical faces. Adapted with permission.^[233] Copyright 2009, American Institute of Physics.

complexed mesostructures^[31] or stimuli-responsive smart devices.^[37,238] These dynamic architectures are defined as 4D structures, with the time-dependent morphology change being the fourth dimension after the original 3D architecting.^[45,239] The rolled-up nanotechnology also plays an essential role in these structures, as the mismatched strains generated during the environment change are utilized to trigger the fourth dimensional transforming.^[31]

5.3.1. 4D Printing

Although 3D printing techniques serve to form structures with great complexity, there are still some architectures that are difficult to print directly.^[240] 4D printing uses 3D printing to fabricate a bilayer or multilayer structure with different materials

which response distinctively to the environmental change, leading to the morphological change of the original 3D structures and the eventual formation of 4D structures. Typical rolling or bending mechanism utilized in 4D printing includes swelling strain and thermal response strain.^[31]

An example of 4D printing utilizing swelling strain is based on hydrogel composite ink.^[81] The hydrogel composite ink contains cellulose fibrils, which undergo shear-induced alignment during printing,^[241] leading to printed filaments with anisotropic stiffness. As shown in Figure 19a-i, the filaments exhibit swelling behavior in the longitudinal direction compared to the transverse direction.^[81,242] Thus, when the filaments in the top and bottom layers are printed in the perpendicular direction, they exhibit different swelling behavior upon contacting with water, inducing a mismatched strain, which leads to the bending of the original structures. The

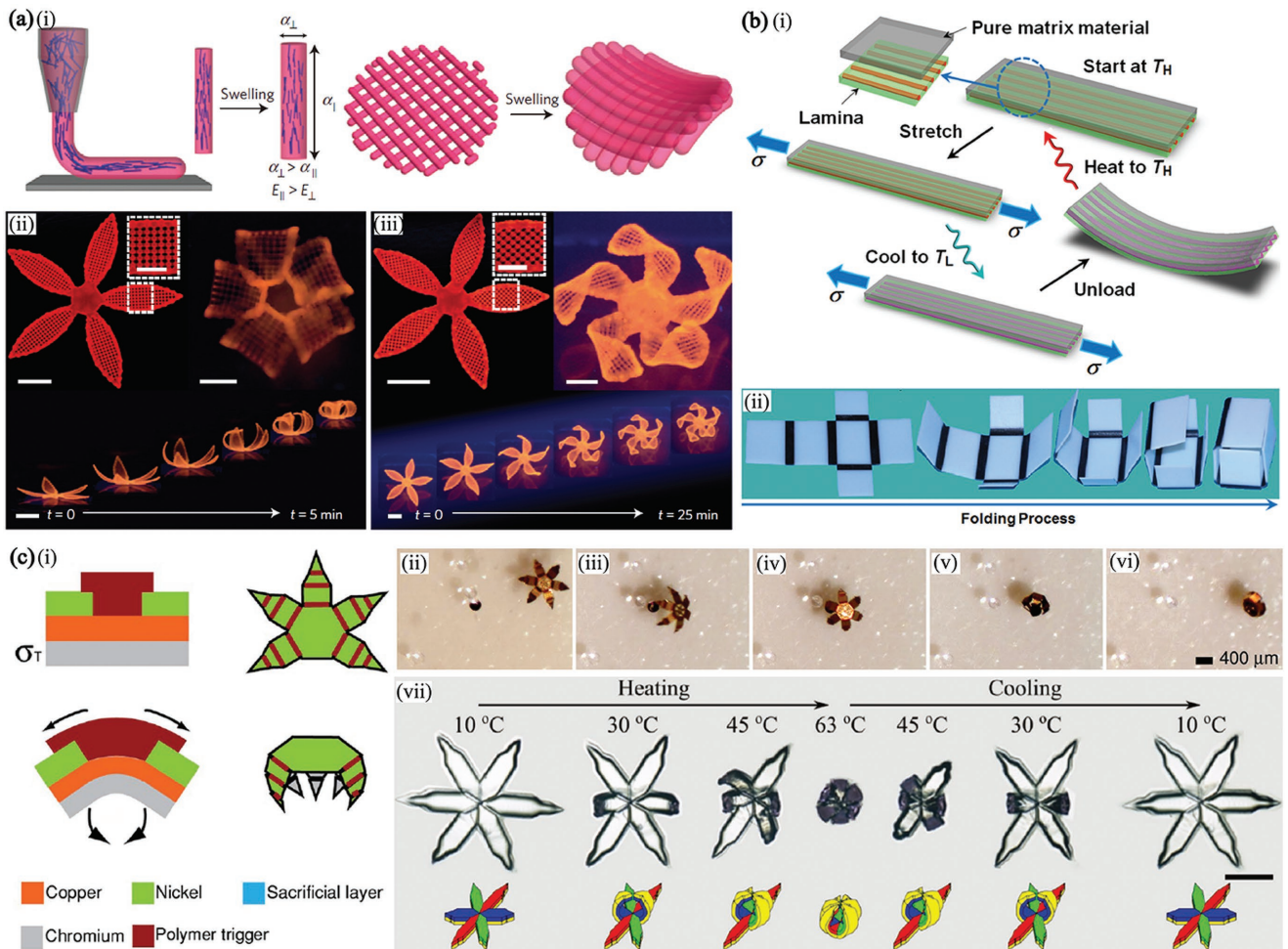


Figure 19. 4D mesostructures demonstrated using rolling mechanism, including 4D printing and stimuli-responsive smart devices. a) 4D printing based on swelling strain and hydrogel composite ink. (i) Schematic diagram showing the shear-induced alignment of cellulose fibrils during direct ink writing and subsequent effects on anisotropic stiffness E and swelling strain α . (ii,iii) 3D flower-like mesostructures fabricated via 4D printing utilizing swelling strain (scale bars: 5 mm; inset = 2.5 mm). Adapted with permission.^[81] Copyright 2016, Macmillan Publishers Limited. b) 4D printing based on thermal-responsive strain and SMP. (i) Illustration of the laminate and matrix structures. After printing, heating, stretching, cooling, and releasing, the thermal response strain induces the bending of the original structures. (ii) Self-assembly of an origami closed box using the combination of laminate and matrix as the flexible hinges. Adapted with permission.^[247] Copyright 2013, AIP Publishing. c) Stimuli-responsive smart devices utilizing rolling mechanism. (i) Schematic diagram showing the on-demand actuation mechanism of microgrippers. (ii–vi) A sequence of optical microscopy images showing the remote-controlled, thermally triggered capture of a dye bead (275 μm) from among several clear beads. (i–vi) Adapted with permission.^[249] Copyright 2009, The National Academy of Sciences of the USA. (vii) Optical images and illustrations of four-state shape changes of grippers during heating and cooling (scale bar: 2 mm). Reproduced with permission.^[250] Copyright 2017, Wiley-VCH.

curvature of the final morphology depends on the swelling ratio, thickness ratio, and elastic properties of two layers,^[243,244] and could be described by the Timoshenko formula. In this way, a mathematical model quantifying all these parameters could be built, providing precise prediction of the final morphology.^[81] The mesostructures fabricated using this method are shown in Figure 19a-ii,iii.

For 4D printing utilizing thermal response strain, shape memory polymer (SMP)^[239,245–247] with tailored thermo-mechanical behavior is used. As shown in Figure 19b-i,^[247] the bilayer in the original 3D printing consists of a matrix exhibiting no shape memory and a laminate architecture containing SMP fibers. When external force is loaded to the bilayer system following by cooling, the different thermal

response of the matrix and laminate leads to a mismatched strain between the two layers. Upon releasing of the external loading, the bilayer would bend into 3D complex structures depending on the fiber architecture. By changing design variables such as composite geometries and properties, the applied mechanical load and the thermal history, various mesostructures could be made from a single flat rectangular strip using this method.^[247] It should be noted that these mesostructures could recover to its original shape upon reheating, thus the shape changing process is reversible. Additionally, such combination of laminate and matrix could be used as flexible hinges between rigid segments, and self-assembly of 3D complex structures based on that have been demonstrated (Figure 19b-ii).^[247]

5.3.2. Stimuli-Responsive Smart Devices

Stimuli-responsive smart devices exhibit the ability to manipulate their morphologies and structures in response to a specific environment change or stimulus such as heat, chemicals, pH, electric field, and light.^[53,238,248] The polyhedron mentioned before with temperature-sensitive polymer at the flexible hinges is a typical smart device, as it exhibits on-demand self-assembly by temperature change.^[226] A further manipulation of the 2D precursor design results in the demonstration of stimuli-responsive microgrippers.^[249] As shown in Figure 19c-i, the polymer trigger is a cresol novolac resin, the mechanical properties of which alters when heated. A sequence of optical microscopy images showing the thermally triggered capture of a dyed bead among several clear beads by the grippers is shown in Figure 19c-ii-vi.^[249] Furthermore, chemicals including organic solvents and caustics that could dissolve or cause delamination of the polymer layer can also actuate the grippers. Such chemical sensitivity of the microgrippers is beneficial for biological applications, as some biochemicals are also proved to be able to trigger the grippers. Additionally, multitemperature-responsive smart devices (Figure 19c-viii)^[250] have also been demonstrated utilizing a bilayer structure of poly[oligo(ethylene glycol) methyl ether methacrylate] gels^[251,252] that swell at three different temperatures due to the varying side chain length and extent of copolymerization.

Other environment parameters have also been used to trigger the stimuli response of devices. For example, Ye et al.^[253] reported the self-rolling and unrolling behavior of biopolymer in response to the pH change. The pH-responsive property is made possible by a sandwich structure of an active silk I layer in the middle of β -sheet silk II and PS layers. The active interlayer exhibits significant change in swelling behavior upon the change of pH, resulting in the pH-responsive reversible rolling. Furthermore, Zhang et al.^[254] have demonstrated an optically responsive programmable smart device utilizing composites of poly(N-isopropylacrylamide) loaded with single-walled carbon nanotubes. The ability of ultrafast near-infrared optical response under laser excitation is enabled by the strong absorption of nanotubes.^[255,256] Other mechanisms such as the photo-n-induced bending of polymer films^[257] might also be utilized to demonstrate optically responsive smart devices in the future.

6. Summary and Outlook

In this review, we have summarized the fabrication methods and recent progress of rolling planar designs into 3D nanostructures. Rolled-up nanotechnology enables a versatile and convenient method to fabricate tubular structures of well-defined geometry. A broad range of materials, including metals, oxides, semiconductors, polymers, and 2D materials have been explored in fabricating 3D tubular micro/nanostructures with extraordinary functionalities. Recent advances based on rolled-up functional devices have extended their applications to a variety of fields, including novel sensors, bioplatforms, environmental remediation, and integrated biomedical devices.

Despite the rapid development and tremendous progress of rolled-up nanotechnology, there remains some technical

challenges before realizing the full potential of multitask systems based on rolled-up platforms. One major challenge lies in the manufacture and control of rolled-up tubular structures. So far, each materials system and corresponding fabrication process has its own limitations. MBE or XOI systems produce single-crystalline nanomembranes of highest purity, but the corrosive etchants limit the materials choices. Fabricating nanomembranes on polymers overcame this issue, but the amorphous materials had inferior quality, which is detrimental to its further applications. In order to bring this area forward, it is challenging but rewarding to develop revolutionary approaches to fabricate complex tubular devices comprising multiple materials with excellent performances.

Another challenge is fabricating high-quality micro- and nanotubes based on 2D materials. The emerging family of 2D materials has become a leading topic in materials research. 2D materials as well as their combinations as van der Waals heterostructures have unique physical properties that enable novel designs of nanodevices and flexible electronics.^[258–261] However, to date only limited progress has been made toward experimental realization of rolling up 2D materials into 3D tubular architectures, in which the materials category and quality need to be further improved. The difficulty of rolling up high-quality 2D materials into functional devices and control over its geometry remains a primary barrier for future development due to the fragility and reactive nature of layered materials. A number of 2D materials and their heterostructures are yet to be explored as building blocks of complex 3D nanostructures. Nevertheless, the fascinating properties and promising prospects of rolled-up nanotechnology offer great opportunities for increasingly sophisticated devices and will continue to develop amazing 3D integrated systems in the future.

Acknowledgements

This work was supported by the Natural Science Foundation of China (Grant Nos. 51711540298, 61628401, U1632115, and 51475093), Science and Technology Commission of Shanghai Municipality (Grant Nos. 17JC1401700 and 18ZR1405100), the National Key Technologies R&D Program of China (Grant No. 2015ZX02102-003), and the Changjiang Young Scholars Program of China.

Conflict of Interest

The authors declare no conflict of interest.

Keywords

3D micro/nanoarchitectures, nanomembrane, rolled-up nanotechnology, strain engineering

Received: September 30, 2018

Revised: October 31, 2018

Published online: December 13, 2018

[1] H. C. Ko, M. P. Stoykovich, J. Song, V. Malyarchuk, W. M. Choi, C.-J. Yu, J. B. GeddesIII, J. Xiao, S. Wang, Y. Huang, J. A. Rogers, *Nature* **2008**, *454*, 748.

- [2] B. Y. Ahn, E. B. Duoss, M. J. Motala, X. Guo, S.-I. Park, Y. Xiong, J. Yoon, R. G. Nuzzo, J. A. Rogers, J. A. Lewis, *Science* **2009**, 323, 1590.
- [3] S. Xu, Z. Yan, K.-I. Jang, W. Huang, H. Fu, J. Kim, Z. Wei, M. Flavin, J. McCracken, R. Wang, A. Badea, Y. Liu, D. Xiao, G. Zhou, J. Lee, H. U. Chung, H. Cheng, W. Ren, A. Banks, X. Li, U. Paik, R. G. Nuzzo, Y. Huang, Y. Zhang, J. A. Rogers, *Science* **2015**, 347, 154.
- [4] Z. Yan, F. Zhang, F. Liu, M. Han, D. Ou, Y. Liu, Q. Lin, X. Guo, H. Fu, Z. Xie, M. Gao, Y. Huang, J. Kim, Y. Qiu, K. Nan, J. Kim, P. Gutruf, H. Luo, A. Zhao, K.-C. Hwang, Y. Huang, Y. Zhang, J. A. Rogers, *Sci. Adv.* **2016**, 2, e1601014.
- [5] T. Ergin, N. Stenger, P. Brenner, J. B. Pendry, M. Wegener, *Science* **2010**, 328, 337.
- [6] J. K. Gansel, M. Thiel, M. S. Rill, M. Decker, K. Bade, V. Saile, G. von Freymann, S. Linden, M. Wegener, *Science* **2009**, 325, 1513.
- [7] C. M. Soukoulis, M. Wegener, *Nat. Photonics* **2011**, 5, 523.
- [8] M. Deubel, G. von Freymann, M. Wegener, S. Pereira, K. Busch, C. M. Soukoulis, *Nat. Mater.* **2004**, 3, 444.
- [9] J. Valentine, S. Zhang, T. Zentgraf, E. Ulin-Avila, D. A. Genov, G. Bartal, X. Zhang, *Nature* **2008**, 455, 376.
- [10] G. von Freymann, A. Ledermann, M. Thiel, I. Staude, S. Essig, K. Busch, M. Wegener, *Adv. Funct. Mater.* **2010**, 20, 1038.
- [11] X. Yu, L. L. Goddard, J. Zhu, X. Li, X. Chen, *Appl. Phys. Lett.* **2018**, 112, 021108.
- [12] L. R. Meza, S. Das, J. R. Greer, *Science* **2014**, 345, 1322.
- [13] D. Jang, L. R. Meza, F. Greer, J. R. Greer, *Nat. Mater.* **2013**, 12, 893.
- [14] D. W. Yee, M. D. Schulz, R. H. Grubbs, J. R. Greer, *Adv. Mater.* **2017**, 29, 1605293.
- [15] X. Zheng, W. Smith, J. Jackson, B. Moran, H. Cui, D. Chen, J. Ye, N. Fang, N. Rodriguez, T. Weisgraber, C. M. Spadaccini, *Nat. Mater.* **2016**, 15, 1100.
- [16] S. Babaee, J. Shim, J. C. Weaver, E. R. Chen, N. Patel, K. Bertoldi, *Adv. Mater.* **2013**, 25, 5044.
- [17] M. Huang, F. Cavallo, F. Liu, M. G. Lagally, *Nanoscale* **2011**, 3, 96.
- [18] L. Dong, L. Zhang, D. J. Bell, D. Grützmacher, B. J. Nelson, *J. Phys.: Conf. Ser.* **2007**, 61, 257.
- [19] J. Rogers, Y. Huang, O. G. Schmidt, D. H. Gracias, *MRS Bull.* **2016**, 41, 123.
- [20] X. Ning, H. Wang, X. Yu, J. A. N. T. Soares, Z. Yan, K. Nan, G. Velarde, Y. Xue, R. Sun, Q. Dong, H. Luan, C. M. Lee, A. Chempakasseril, M. Han, Y. Wang, L. Li, Y. Huang, Y. Zhang, J. A. Rogers, *Adv. Funct. Mater.* **2017**, 27, 1605914.
- [21] M. A. Skylar-Scott, S. Gunasekaran, J. A. Lewis, *Proc. Natl. Acad. Sci. USA* **2016**, 113, 6137.
- [22] J. F. Destino, N. A. Dudukovic, M. A. Johnson, D. T. Nguyen, T. D. Yee, G. C. Egan, A. M. Sawvel, W. A. Steele, T. F. Baumann, E. B. Duoss, T. Suratwala, R. Dylla-Spears, *Adv. Mater. Technol.* **2018**, 3, 1700323.
- [23] A. Vyatskikh, S. Delalande, A. Kudo, X. Zhang, C. M. Portela, J. R. Greer, *Nat. Commun.* **2018**, 9, 593.
- [24] B. H. Cumpston, S. P. Ananthavel, S. Barlow, D. L. Dyer, J. E. Ehrlich, L. L. Erskine, A. A. Heikal, S. M. Kuebler, I.-Y. S. Lee, D. McCord-Maughon, J. Qin, H. Röckel, M. Rumi, X.-L. Wu, S. R. Marder, J. W. Perry, *Nature* **1999**, 398, 51.
- [25] S. Kawata, H.-B. Sun, T. Tanaka, K. Takada, *Nature* **2001**, 412, 697.
- [26] C. N. LaFratta, J. T. Fourkas, T. Baldacchini, R. A. Farrer, *Angew. Chem., Int. Ed.* **2007**, 46, 6238.
- [27] W. Chu, Y. Tan, P. Wang, J. Xu, W. Li, J. Qi, Y. Cheng, *Adv. Mater. Technol.* **2018**, 3, 1700396.
- [28] X. Zheng, H. Lee, T. H. Weisgraber, M. Shusteff, J. DeOtte, E. B. Duoss, J. D. Kuntz, M. M. Biener, Q. Ge, J. A. Jackson, S. O. Kucheyev, N. X. Fang, C. M. Spadaccini, *Science* **2014**, 344, 1373.
- [29] W. Gao, S. Sattayasamitsathit, J. Orozco, J. Wang, *J. Am. Chem. Soc.* **2011**, 133, 11862.
- [30] J. Li, I. Rozen, J. Wang, *ACS Nano* **2016**, 10, 5619.
- [31] Y. Zhang, F. Zhang, Z. Yan, Q. Ma, X. Li, Y. Huang, J. A. Rogers, *Nat. Rev. Mater.* **2017**, 2, 17019.
- [32] X. Zhang, C. Sun, N. Fang, *J. Nanopart. Res.* **2004**, 6, 125.
- [33] J. A. Rogers, M. G. Lagally, R. G. Nuzzo, *Nature* **2011**, 477, 45.
- [34] S. Pandey, M. Ewing, A. Kunas, N. Nguyen, D. H. Gracias, G. Menon, *Proc. Natl. Acad. Sci. USA* **2011**, 108, 19885.
- [35] D. H. Gracias, V. Kavthekar, J. C. Love, K. E. Paul, G. M. Whitesides, *Adv. Mater.* **2002**, 14, 235.
- [36] Z. Yan, F. Zhang, J. Wang, F. Liu, X. Guo, K. Nan, Q. Lin, M. Gao, D. Xiao, Y. Shi, Y. Qiu, H. Luan, J. H. Kim, Y. Wang, H. Luo, M. Han, Y. Huang, Y. Zhang, J. A. Rogers, *Adv. Funct. Mater.* **2016**, 26, 2629.
- [37] L. Xu, T. C. Shyu, N. A. Kotov, *ACS Nano* **2017**, 11, 7587.
- [38] H. Fu, K. Nan, P. Froeter, W. Huang, Y. Liu, Y. Wang, J. Wang, Z. Yan, H. Luan, X. Guo, Y. Zhang, C. Jiang, L. Li, A. C. Dunn, X. Li, Y. Huang, Y. Zhang, J. A. Rogers, *Small* **2017**, 13, 1700151.
- [39] H. Fu, K. Nan, W. Bai, W. Huang, K. Bai, L. Lu, C. Zhou, Y. Liu, F. Liu, J. Wang, M. Han, Z. Yan, H. Luan, Y. Zhang, Y. Zhang, J. Zhao, X. Cheng, M. Li, J. W. Lee, Y. Liu, D. Fang, X. Li, Y. Huang, Y. Zhang, J. A. Rogers, *Nat. Mater.* **2018**, 17, 268.
- [40] A. M. Abdullah, X. Li, P. V. Braun, J. A. Rogers, K. J. Hsia, *Adv. Mater.* **2018**, 30, 1801669.
- [41] G. Huang, Y. Mei, *Adv. Mater.* **2012**, 24, 2517.
- [42] M. Huang, C. Boone, M. Roberts, D. E. Savage, L. Lagally, N. Shaji, H. Qin, R. Blick, J. A. Nairn, F. Liu, *Adv. Mater.* **2005**, 17, 2860.
- [43] J. Zhang, J. Li, S. Tang, Y. Fang, J. Wang, G. Huang, R. Liu, L. Zheng, X. Cui, Y. Mei, *Sci. Rep.* **2015**, 5, 15012.
- [44] Y. Zhang, D. Han, D. Du, G. Huang, T. Qiu, Y. Mei, *Plasmonics* **2015**, 10, 949.
- [45] G. Huang, Y. Mei, *Small* **2018**, 14, 1703665.
- [46] Z. Chen, G. Huang, I. Trase, X. Han, Y. Mei, *Phys. Rev. Appl.* **2016**, 5, 017001.
- [47] Q. Guo, Z. Di, M. G. Lagally, Y. Mei, *Mater. Sci. Eng., R* **2018**, 128, 1.
- [48] O. G. Schmidt, K. Eberl, *Nature* **2001**, 410, 168.
- [49] V. Luchnikov, O. Sydorenko, M. Stamm, *Adv. Mater.* **2005**, 17, 1177.
- [50] E. Vekris, G. A. Ozin, V. Kitaev, *Adv. Mater.* **2006**, 18, 2481.
- [51] Y. Mei, G. Huang, A. A. Solovev, E. B. Ureña, I. Mönch, F. Ding, T. Reindl, R. K. Y. Fu, P. K. Chu, O. G. Schmidt, *Adv. Mater.* **2008**, 20, 4085.
- [52] J. Li, J. Zhang, W. Gao, G. Huang, D. Di, R. Liu, J. Wang, Y. Mei, *Adv. Mater.* **2013**, 25, 3715.
- [53] B. Xu, Z. Tian, J. Wang, H. Han, T. Lee, Y. Mei, *Sci. Adv.* **2018**, 4, eaap8203.
- [54] Z. Tian, L. Zhang, Y. Fang, B. Xu, S. Tang, N. Hu, Z. An, Z. Chen, Y. Mei, *Adv. Mater.* **2017**, 29, 1604572.
- [55] O. G. Schmidt, C. Deneke, Y. M. Manz, C. Müller, *Phys. E* **2002**, 13, 969.
- [56] L. Zhang, L. Dong, B. J. Nelson, *Appl. Phys. Lett.* **2008**, 92, 143110.
- [57] L. Zhang, J. J. Abbott, L. Dong, K. E. Peyer, B. E. Kratochvil, H. Zhang, C. Bergeles, B. J. Nelson, *Nano Lett.* **2009**, 9, 3663.
- [58] W. Li, G. Huang, J. Wang, Y. Yu, X. Wu, X. Cui, Y. Mei, *Lab Chip* **2012**, 12, 2322.
- [59] Z. Tian, W. Huang, B. Xu, X. Li, Y. Mei, *Nano Lett.* **2018**, 18, 3688.
- [60] S. Böttner, M. R. Jorgensen, O. G. Schmidt, *Scr. Mater.* **2016**, 122, 119.
- [61] X. Lin, Y. Fang, L. Zhu, J. Zhang, G. Huang, J. Wang, Y. Mei, *Adv. Opt. Mater.* **2016**, 4, 936.
- [62] H. Wang, S. Li, H. Zhen, X. Nie, G. Huang, Y. Mei, W. Lu, *J. Semicond.* **2017**, 38, 054006.
- [63] H. Wang, H. Zhen, S. Li, Y. Jing, G. Huang, Y. Mei, W. Lu, *Sci. Adv.* **2016**, 2, e1600027.
- [64] H. Ning, Y. Zhang, H. Zhu, A. Ingham, G. Huang, Y. Mei, A. A. Solovev, *Micromachines* **2018**, 9, 75.

- [65] Y. Zhang, H. Zhu, W. Qiu, Y. Zhou, G. Huang, Y. Mei, A. A. Solovev, *Chem. Commun.* **2018**, *54*, 5692.
- [66] G. Huang, J. Wang, Z. Liu, D. Zhou, Z. Tian, B. Xu, L. Li, Y. Mei, *Nanoscale* **2017**, *9*, 18590.
- [67] J. Deng, X. Lu, L. Liu, L. Zhang, O. G. Schmidt, *Adv. Energy Mater.* **2016**, *6*, 1600797.
- [68] B. Xu, B. Zhang, L. Wang, G. Huang, Y. Mei, *Adv. Funct. Mater.* **2018**, *28*, 1705872.
- [69] L. Soler, V. Magdanz, V. M. Fomin, S. Sanchez, O. G. Schmidt, *ACS Nano* **2013**, *7*, 9611.
- [70] V. Y. Prinz, V. A. Seleznev, A. K. Gutakovskiy, A. V. Chehovskiy, V. V. Preobrazhenskii, M. A. Putyato, T. A. Gavrilova, *Phys. E* **2000**, *6*, 828.
- [71] O. G. Schmidt, N. Y. Jin-Phillipp, *Appl. Phys. Lett.* **2001**, *78*, 3310.
- [72] X. Li, *Adv. Opt. Photonics* **2011**, *3*, 366.
- [73] S. V. Golod, V. Y. Prinz, P. Wägli, L. Zhang, O. Kirfel, E. Deckhardt, F. Glaus, C. David, D. Grützmacher, *Appl. Phys. Lett.* **2004**, *84*, 3391.
- [74] L. Zhang, E. Ruh, D. Grützmacher, L. Dong, D. J. Bell, B. J. Nelson, C. Schönenberger, *Nano Lett.* **2006**, *6*, 1311.
- [75] F. Cavallo, W. Sigle, O. G. Schmidt, *J. Appl. Phys.* **2008**, *103*, 116103.
- [76] Y. C. Tsui, T. W. Clyne, *Thin Solid Films* **1997**, *306*, 23.
- [77] X. Yu, E. Arbabi, L. L. Goddard, X. Li, X. Chen, *Appl. Phys. Lett.* **2015**, *107*, 031102.
- [78] X. Yu, L. L. Goddard, X. Li, X. Chen, *Appl. Phys. Lett.* **2016**, *109*, 111104.
- [79] J. M. Olson, *Mater. Sci. Semicond. Process.* **2002**, *5*, 51.
- [80] M. F. Doerner, W. D. Nix, *Crit. Rev. Solid State Mater. Sci.* **1988**, *14*, 225.
- [81] A. S. Gladman, E. A. Matsumoto, R. G. Nuzzo, L. Mahadevan, J. A. Lewis, *Nat. Mater.* **2016**, *15*, 413.
- [82] D.-Y. Khang, H. Jiang, Y. Huang, J. A. Rogers, *Science* **2006**, *311*, 208.
- [83] F. Banhart, *Rep. Prog. Phys.* **1999**, *62*, 1181.
- [84] D. Ugarte, *Nature* **1992**, *359*, 707.
- [85] J.-W. Liu, J. Xu, Y. Ni, F.-J. Fan, C.-L. Zhang, S.-H. Yu, *ACS Nano* **2012**, *6*, 4500.
- [86] R. Ramachandran, D. Johnson-McDaniel, T. T. Salguero, *Chem. Mater.* **2016**, *28*, 7257.
- [87] J. Zang, M. Huang, F. Liu, *Phys. Rev. Lett.* **2007**, *98*, 146102.
- [88] F. Liu, M. G. Lagally, *Phys. Rev. Lett.* **1996**, *76*, 3156.
- [89] V. Zielasek, F. Liu, Y. Zhao, J. B. Maxson, M. G. Lagally, *Phys. Rev. B* **2001**, *64*, 201320.
- [90] S. Tanaka, C. C. Umbach, J. M. Blakely, R. M. Tromp, M. Mankos, *Appl. Phys. Lett.* **1996**, *69*, 1235.
- [91] J.-H. Cho, A. Azam, D. H. Gracias, *Langmuir* **2010**, *26*, 16534.
- [92] J. Huang, M. Juszkiewicz, W. H. de Jeu, E. Cerdá, T. Emrick, N. Menon, T. P. Russell, *Science* **2007**, *317*, 650.
- [93] J. H. Cho, T. James, D. H. Gracias, *Adv. Mater.* **2010**, *22*, 2320.
- [94] J. H. Cho, D. Datta, S. Y. Park, V. B. Shenoy, D. H. Gracias, *Nano Lett.* **2010**, *10*, 5098.
- [95] X. Li, *J. Phys. D: Appl. Phys.* **2008**, *41*, 193001.
- [96] M. Watari, J. Galbraith, H. P. Lang, M. Sousa, M. Hegner, C. Gerber, M. A. Horton, R. A. McKendry, *J. Am. Chem. Soc.* **2007**, *129*, 601.
- [97] X. Xie, L. Ju, X. Feng, Y. Sun, R. Zhou, K. Liu, S. Fan, Q. Li, K. Jiang, *Nano Lett.* **2009**, *9*, 2565.
- [98] C. Py, P. Reverdy, L. Doppler, J. Bico, B. Roman, C. N. Baroud, *Phys. Rev. Lett.* **2007**, *98*, 156103.
- [99] X. Guo, H. Li, B. Yeop Ahn, E. B. Duoss, K. J. Hsia, J. A. Lewis, R. G. Nuzzo, *Proc. Natl. Acad. Sci. USA* **2009**, *106*, 20149.
- [100] V. P. Tolstoy, L. B. Gulina, *J. Nano-Electron. Phys.* **2013**, *5*, 2012.
- [101] V. E. Gurenko, V. P. Tolstoy, L. B. Gulina, *Nanosyst.: Phys., Chem., Math.* **2017**, *8*, 471.
- [102] D. Yu, F. Liu, *Nano Lett.* **2007**, *7*, 3046.
- [103] M. Calvaresi, M. Quintana, P. Rudolf, F. Zerbetto, M. Prato, *ChemPhysChem* **2013**, *14*, 3447.
- [104] A. Sidorov, D. Mudd, G. Sumanasekera, P. J. Ouseph, C. S. Jayanthi, S. Y. Wu, *Nanotechnology* **2009**, *20*, 055611.
- [105] D. Xia, Q. Xue, J. Xie, H. Chen, C. Lv, *Comput. Mater. Sci.* **2010**, *49*, 588.
- [106] S. Kang, J. B. Pyo, T. S. Kim, *Langmuir* **2018**, *34*, 5831.
- [107] L. M. Viculis, J. J. Mack, R. B. Kaner, *Science* **2003**, *299*, 1361.
- [108] H. Shioyama, T. Akita, *Carbon* **2003**, *41*, 179.
- [109] M. V. Savoskin, V. N. Mochalin, A. P. Yaroshenko, N. I. Lazareva, T. E. Konstantinova, I. V. Barsukov, I. G. Prokofiev, *Carbon* **2007**, *45*, 2797.
- [110] S. Wang, L. Ai, Q. Bao, M. Lin, S. Deng, B. M. Goh, K. P. Loh, *J. Am. Chem. Soc.* **2009**, *131*, 16832.
- [111] X. Wang, D.-P. Yang, G. Huang, P. Huang, G. Shen, S. Guo, Y. Mei, D. Cui, *J. Mater. Chem.* **2012**, *22*, 17441.
- [112] G. S. Huang, Y. F. Mei, F. Cavallo, S. Baunack, E. Coric, T. Gemming, F. Bertram, J. Christen, R. K. Y. Fu, P. K. Chu, O. G. Schmidt, *J. Appl. Phys.* **2009**, *105*, 016103.
- [113] Y. Mei, A. A. Solovev, S. Sanchez, O. G. Schmidt, *Chem. Soc. Rev.* **2011**, *40*, 2109.
- [114] P. O. Vaccaro, K. Kubota, T. Aida, *Appl. Phys. Lett.* **2001**, *78*, 2852.
- [115] S. Mendach, R. Songmuang, S. Kiravittaya, A. Rastelli, M. Benyoucef, O. G. Schmidt, *Appl. Phys. Lett.* **2006**, *88*, 111120.
- [116] D. J. Bell, L. Dong, B. J. Nelson, M. Golling, L. Zhang, D. Grützmacher, *Nano Lett.* **2006**, *6*, 725.
- [117] D. J. Thurmer, C. Deneke, Y. Mei, O. G. Schmidt, *Appl. Phys. Lett.* **2006**, *89*, 223507.
- [118] N. Shaji, H. Qin, R. H. Blick, L. J. Klein, C. Deneke, O. G. Schmidt, *Appl. Phys. Lett.* **2007**, *90*, 042101.
- [119] S. Mendach, S. Kiravittaya, A. Rastelli, M. Benyoucef, R. Songmuang, O. G. Schmidt, *Phys. Rev. B* **2008**, *78*, 035317.
- [120] C. Streloew, C. M. Schultz, H. Rehberg, H. Welsch, C. Heyn, D. Heitmann, T. Kipp, *Phys. Rev. B* **2007**, *76*, 045303.
- [121] I. S. Chun, K. Bassett, A. Challa, X. Li, *Appl. Phys. Lett.* **2010**, *96*, 251106.
- [122] O. G. Schmidt, N. Schmarje, C. Deneke, C. Müller, N. Y. Jin-Phillipp, *Adv. Mater.* **2001**, *13*, 756.
- [123] R. Songmuang, A. Rastelli, S. Mendach, O. G. Schmidt, *Appl. Phys. Lett.* **2007**, *90*, 091905.
- [124] R. Songmuang, C. Deneke, O. G. Schmidt, *Appl. Phys. Lett.* **2006**, *89*, 223109.
- [125] W. Huang, X. Yu, P. Froeter, R. Xu, P. Ferreira, X. Li, *Nano Lett.* **2012**, *12*, 6283.
- [126] P. Froeter, X. Yu, W. Huang, F. Du, M. Li, I. Chun, S. H. Kim, K. J. Hsia, J. A. Rogers, X. Li, *Nanotechnology* **2013**, *24*, 475301.
- [127] P. Froeter, Y. Huang, O. V. Cangellaris, W. Huang, E. W. Dent, M. U. Gillette, J. C. Williams, X. Li, *ACS Nano* **2014**, *8*, 11108.
- [128] W. Huang, J. Zhou, P. J. Froeter, K. Walsh, S. Liu, M. D. Kraman, M. Li, J. A. Michaels, D. J. Sievers, S. Gong, X. Li, *Nat. Electron.* **2018**, *1*, 305.
- [129] F. Wang, Y. Shi, J. Liu, Y. Lu, S. Gu, Y. Zheng, *J. Electrochem. Soc.* **1997**, *144*, L37.
- [130] D. Grützmacher, L. Zhang, L. Dong, D. Bell, B. Nelson, A. Prinz, E. Ruh, *Microelectron. J.* **2008**, *39*, 478.
- [131] R. Songmuang, N. Y. Jin-Phillipp, S. Mendach, O. G. Schmidt, *Appl. Phys. Lett.* **2006**, *88*, 021913.
- [132] F. Cavallo, R. Songmuang, O. G. Schmidt, *Appl. Phys. Lett.* **2008**, *93*, 143113.
- [133] C. Deneke, U. Zschieschang, H. Klauk, O. G. Schmidt, *Appl. Phys. Lett.* **2006**, *89*, 263110.
- [134] N. Y. Jin-Phillipp, J. Thomas, M. Kelsch, C. Deneke, R. Songmuang, O. G. Schmidt, *Appl. Phys. Lett.* **2006**, *88*, 033113.

- [135] C. Deneke, C. Müller, N. Y. Jin-Phillipp, O. G. Schmidt, *Semicond. Sci. Technol.* **2002**, *17*, 1278.
- [136] L. Zhang, E. Deckhardt, A. Weber, C. Schönenberger, D. Grützmacher, *Nanotechnology* **2005**, *16*, 655.
- [137] I. S. Chun, X. Li, *IEEE Trans. Nanotechnol.* **2008**, *7*, 493.
- [138] F. Liu, M. G. Lagally, J. Zang, *MRS Bull.* **2009**, *34*, 190.
- [139] S. V. Golod, V. Y. Prinz, V. I. Mashanov, A. K. Gutakovskiy, *Semicond. Sci. Technol.* **2001**, *16*, 181.
- [140] S. Nakaharai, T. Tezuka, N. Sugiyama, Y. Moriyama, S. I. Takagi, *Appl. Phys. Lett.* **2003**, *83*, 3516.
- [141] T. Tezuka, N. Sugiyama, S. Takagi, *Appl. Phys. Lett.* **2001**, *79*, 1798.
- [142] F. Cavallo, R. Songmuang, C. Ulrich, O. G. Schmidt, *Appl. Phys. Lett.* **2007**, *90*, 193120.
- [143] J. R. Schwank, *Microelectron. Eng.* **1997**, *36*, 335.
- [144] O. Faynot, T. Poiroux, F. Andrieu, C. Jahan, S. Barraud, T. Ernst, L. Brevard, S. Deleonibus, *Proc. Int. Work. Junction Technol.* **2006**, *200*.
- [145] Q. Guo, M. Zhang, Z. Xue, J. Zhang, G. Wang, D. Chen, Z. Mu, G. Huang, Y. Mei, Z. Di, X. Wang, *AIP Adv.* **2015**, *5*, 037115.
- [146] Q. Guo, G. Wang, D. Chen, G. Li, G. Huang, M. Zhang, X. Wang, Y. Mei, Z. Di, *Appl. Phys. Lett.* **2017**, *110*, 112104.
- [147] P. G. Evans, D. S. Tinberg, M. M. Roberts, M. G. Lagally, Y. Xiao, B. Lai, Z. Cai, *Appl. Phys. Lett.* **2005**, *87*, 073112.
- [148] Z. Tian, B. Xu, B. Hsu, L. Stan, Z. Yang, Y. Mei, *Nano Lett.* **2018**, *18*, 3017.
- [149] X. Wu, Z. Tian, H. Cong, Y. Wang, R. Edy, G. Huang, Z. Di, C. Xue, Y. Mei, *Nanotechnology* **2018**, *29*, 42LT02.
- [150] S. Wirths, R. Geiger, N. von den Driesch, G. Mussler, T. Stoica, S. Mantl, Z. Ikonik, M. Luysberg, S. Chiussi, J. M. Hartmann, H. Sigg, J. Faist, D. Buca, D. Grützmacher, *Nat. Photonics* **2015**, *9*, 88.
- [151] S. Su, B. Cheng, C. Xue, W. Wang, Q. Cao, H. Xue, W. Hu, G. Zhang, Y. Zuo, Q. Wang, *Opt. Express* **2011**, *19*, 6400.
- [152] Z. Liu, H. Cong, F. Yang, C. Li, J. Zheng, C. Xue, Y. Zuo, B. Cheng, Q. Wang, *Sci. Rep.* **2016**, *6*, 38386.
- [153] M. Oehme, E. Kasper, J. Schulze, *ECS J. Solid State Sci. Technol.* **2013**, *2*, R76.
- [154] Z. Wu, X. Lin, X. Zou, J. Sun, Q. He, *ACS Appl. Mater. Interfaces* **2015**, *7*, 250.
- [155] E. W. H. Jager, E. Smela, O. Inganäs, *Science* **2000**, *290*, 1540.
- [156] K. Kalaitzidou, A. J. Crosby, *Appl. Phys. Lett.* **2008**, *93*, 041910.
- [157] B. Simpson, G. Nunnery, R. Tannenbaum, K. Kalaitzidou, *J. Mater. Chem.* **2010**, *20*, 3496.
- [158] K. Kumar, B. Nandan, V. Luchnikov, E. B. Gowd, M. Stamm, *Langmuir* **2009**, *25*, 7667.
- [159] S. Zakharchenko, N. Puretskiy, G. Stoychev, M. Stamm, L. Ionov, *Soft Matter* **2010**, *6*, 2633.
- [160] S. Zakharchenko, E. Sperling, L. Ionov, *Biomacromolecules* **2011**, *12*, 2211.
- [161] V. Luchnikov, L. Ionov, M. Stamm, *Macromol. Rapid Commun.* **2011**, *32*, 1943.
- [162] B. A. Ganji, B. Y. Majlis, *Microsyst. Technol.* **2010**, *16*, 1803.
- [163] G. Zhao, A. Ambrosi, M. Pumera, *J. Mater. Chem. A* **2014**, *2*, 1219.
- [164] H. Ji, X. Wu, L. Fan, C. Krien, F. Fiering, Y. Guo, Y. Mei, O. G. Schmidt, *Adv. Mater.* **2010**, *22*, 4591.
- [165] A. A. Solovev, Y. Mei, E. B. Ureña, G. Huang, O. G. Schmidt, *Small* **2009**, *5*, 1688.
- [166] H. Pan, Y. Feng, J. Lin, *Phys. Rev. B* **2005**, *72*, 085415.
- [167] Y. Chen, J. Lu, Z. Gao, *J. Phys. Chem. C* **2007**, *111*, 1625.
- [168] G. Mpourmpakis, E. Tylianakis, G. E. Froudakis, *Nano Lett.* **2007**, *7*, 1893.
- [169] X. Shi, Y. Cheng, N. M. Pugno, H. Gao, *Appl. Phys. Lett.* **2010**, *96*, 053115.
- [170] M. M. Fogler, A. H. Castro Neto, F. Guinea, *Phys. Rev. B* **2010**, *81*, 161408.
- [171] C.-H. Chang, C. Ortix, *Nano Lett.* **2017**, *17*, 3076.
- [172] Z. Liu, J. Gao, G. Zhang, Y. Cheng, Y.-W. Zhang, *Nanotechnology* **2017**, *28*, 385704.
- [173] W. Lee, Y. Liu, Y. Lee, B. K. Sharma, S. M. Shinde, S. D. Kim, K. Nan, Z. Yan, M. Han, Y. Huang, Y. Zhang, J.-H. Ahn, J. A. Rogers, *Nat. Commun.* **2018**, *9*, 1417.
- [174] J. Zheng, H. Liu, B. Wu, Y. Guo, T. Wu, G. Yu, Y. Liu, D. Zhu, *Adv. Mater.* **2011**, *23*, 2460.
- [175] F. Zeng, Y. Kuang, Y. Wang, Z. Huang, C. Fu, H. Zhou, *Adv. Mater.* **2011**, *23*, 4929.
- [176] B. Zheng, Z. Xu, C. Gao, *Nanoscale* **2016**, *8*, 1413.
- [177] D. Berman, S. A. Deshmukh, S. K. R. S. Sankaranarayanan, A. Erdemir, A. V. Surnant, *Science* **2015**, *348*, 1118.
- [178] T. Sharifi, E. Gracia-Espino, H. R. Barzegar, X. Jia, F. Nitze, G. Hu, P. Nordblad, C.-W. Tai, T. Wågberg, *Nat. Commun.* **2013**, *4*, 2319.
- [179] E. Perim, L. D. Machado, D. S. Galvao, *Front. Mater.* **2014**, *1*, 31.
- [180] C. A. Amadei, I. Y. Stein, G. J. Silverberg, B. L. Wardle, C. D. Vecitis, *Nanoscale* **2016**, *8*, 6783.
- [181] L. Baptista-Pires, J. Orozco, P. Guardia, A. Merkoçi, *Small* **2018**, *14*, 1702746.
- [182] X. Chen, R. A. Boulos, J. F. Dobson, C. L. Raston, *Nanoscale* **2012**, *5*, 498.
- [183] A. K. Schaper, M. S. Wang, Z. Xu, Y. Bando, D. Golberg, *Nano Lett.* **2011**, *11*, 3295.
- [184] D. Xia, J. Xie, H. Chen, C. Lv, F. Besenbacher, Q. Xue, M. Dong, *Small* **2010**, *6*, 2010.
- [185] O.-K. Park, C. S. Tiwary, Y. Yang, S. Bhowmick, S. Vinod, Q. Zhang, V. L. Colvin, S. A. S. Asif, R. Vajtai, E. S. Penev, B. I. Yakobson, P. M. Ajayan, *Nanoscale* **2017**, *9*, 6991.
- [186] I. D. Barcelos, L. G. Moura, R. G. Lacerda, A. Malachias, *Nano Lett.* **2014**, *14*, 3919.
- [187] G. Mao, Q. Wang, Z. Chai, H. Liu, K. Liu, X. Ren, *RSC Adv.* **2017**, *7*, 14481.
- [188] N. Patra, B. Wang, P. Král, *Nano Lett.* **2009**, *9*, 3766.
- [189] U. Mirsaidov, V. R. S. S. Mokkapati, D. Bhattacharya, H. Andersen, M. Bosman, B. Özyilmaz, P. Matsudaira, *Lab Chip* **2013**, *13*, 2874.
- [190] X. Cui, Z. Kong, E. Gao, D. Huang, Y. Hao, H. Shen, C. Di, Z. Xu, J. Zheng, D. Zhu, *Nat. Commun.* **2018**, *9*, 1301.
- [191] M. Z. Miskin, K. J. Dorsey, B. Bircan, Y. Han, D. A. Muller, P. L. McEuen, I. Cohen, *Proc. Natl. Acad. Sci. USA* **2018**, *115*, 466.
- [192] W. Xu, Z. Qin, C. T. Chen, H. R. Kwag, Q. Ma, A. Sarkar, M. J. Buehler, D. H. Gracias, *Sci. Adv.* **2017**, *3*, e1701084.
- [193] Y. V. Nastaushev, V. Y. Prinz, S. N. Svitashova, *Nanotechnology* **2005**, *16*, 908.
- [194] S. H. Park, G. Yuan, D. Chen, K. Xiong, J. Song, B. Leung, J. Han, *Nano Lett.* **2014**, *14*, 4293.
- [195] G. D. Cole, Y. Bai, M. Aspelmeier, E. A. Fitzgerald, *Appl. Phys. Lett.* **2010**, *96*, 261102.
- [196] H. Kim, C. Kim, M. Yu, H.-S. Kim, R. H. Blick, *J. Appl. Phys.* **2010**, *108*, 074307.
- [197] H. Wang, J. G. S. Moo, M. Pumera, *Nanoscale* **2014**, *6*, 11359.
- [198] P. Cendula, S. Kiravittaya, Y. F. Mei, C. Deneke, O. G. Schmidt, *Phys. Rev. B* **2009**, *79*, 085429.
- [199] F. Cavallo, M. G. Lagally, *Soft Matter* **2010**, *6*, 439.
- [200] Y. P. Zhao, D. X. Ye, G. C. Wang, T. M. Lu, *Nano Lett.* **2002**, *2*, 351.
- [201] A. I. Fedorchenko, A. B. Wang, V. I. Mashanov, W. P. Huang, H. H. Cheng, *Appl. Phys. Lett.* **2006**, *89*, 043119.
- [202] F. Liu, P. Rugheimer, E. Mateeva, D. E. Savage, M. G. Lagally, *Nature* **2002**, *416*, 498.
- [203] F. Liu, M. Huang, P. P. Rugheimer, D. E. Savage, M. G. Lagally, *Phys. Rev. Lett.* **2002**, *89*, 136101.
- [204] S. Timoshenko, *J. Opt. Soc. Am.* **1925**, *11*, 233.
- [205] J. Zang, F. Liu, *Appl. Phys. Lett.* **2008**, *92*, 129.
- [206] S. Alben, B. Balakrishnan, E. Smela, *Nano Lett.* **2011**, *11*, 2280.
- [207] A. B. Vorob, V. Y. Prinz, *Semicond. Sci. Technol.* **2002**, *17*, 614.

- [208] P. Cendula, S. Kiravittaya, I. Mönch, J. Schumann, O. G. Schmidt, *Nano Lett.* **2011**, *11*, 236.
- [209] M. M. Hawkeye, M. J. Brett, *J. Vac. Sci. Technol., A* **2007**, *25*, 1317.
- [210] I. S. Chun, A. Challal, B. Derickson, K. J. Hsia, X. Li, *Nano Lett.* **2010**, *10*, 3927.
- [211] I. S. Chun, V. B. Verma, V. C. Elarde, S. W. Kim, J. M. Zuo, J. J. Coleman, X. Li, *J. Cryst. Growth* **2008**, *310*, 2353.
- [212] W. Huang, S. Koric, X. Yu, K. J. Hsia, X. Li, *Nano Lett.* **2014**, *14*, 6293.
- [213] N. Chouaieb, A. Goriely, J. H. Maddocks, *Proc. Natl. Acad. Sci. USA* **2006**, *103*, 9398.
- [214] Y. Liu, Z. Yan, Q. Lin, X. Guo, M. Han, *Adv. Funct. Mater.* **2016**, *26*, 2909.
- [215] R. M. Erb, J. S. Sander, R. Grisch, A. R. Studart, *Nat. Commun.* **2013**, *4*, 1712.
- [216] L. T. de Haan, J. M. N. Verjans, D. J. Broer, C. W. M. Bastiaansen, A. P. H. J. Schenning, *J. Am. Chem. Soc.* **2014**, *136*, 10585.
- [217] C. Strelow, C. M. Schultz, H. Rehberg, M. Sauer, H. Welsch, A. Stemmann, C. Heyn, D. Heitmann, T. Kipp, *Phys. Rev. B* **2012**, *85*, 155329.
- [218] J. Wang, T. Zhan, G. Huang, P. K. Chu, Y. Mei, *Laser Photonics Rev.* **2014**, *8*, 521.
- [219] E. Moiseeva, Y. M. Senousy, S. McNamara, C. K. Harnett, *J. Micromech. Microeng.* **2007**, *17*, N63.
- [220] K. Chalapat, N. Chekurov, H. Jiang, J. Li, B. Parviz, G. S. Paraoanu, *Adv. Mater.* **2013**, *25*, 91.
- [221] Z. Zhao, X. Kuang, C. Yuan, H. J. Qi, D. Fang, *ACS Appl. Mater. Interfaces* **2018**, *10*, 19932.
- [222] V. Y. Prinz, D. Grutzmacher, A. Beyer, C. David, B. Ketterer, E. Deckardt, *Nanotechnology* **2001**, *12*, 399.
- [223] V. B. Shenoy, D. H. Gracias, *MRS Bull.* **2012**, *37*, 847.
- [224] T. G. Leong, A. M. Zarafshar, D. H. Gracias, *Small* **2010**, *6*, 792.
- [225] T. G. Leong, P. A. Lester, T. L. Koh, E. K. Call, D. H. Gracias, *Langmuir* **2007**, *23*, 8747.
- [226] T. G. Leong, B. R. Benson, E. K. Call, D. H. Gracias, *Small* **2008**, *4*, 1605.
- [227] K. Malachowski, M. Jamal, Q. Jin, B. Polat, C. J. Morris, D. H. Gracias, *Nano Lett.* **2014**, *14*, 4164.
- [228] T. G. Leong, C. L. Randall, B. R. Benson, A. M. Zarafshar, D. H. Gracias, *Lab Chip* **2008**, *8*, 1621.
- [229] W. J. Arora, A. J. Nichol, H. I. Smith, G. Barbastathis, *Appl. Phys. Lett.* **2006**, *88*, 053108.
- [230] J. A. Thornton, D. W. Hoffman, *Thin Solid Films* **1989**, *171*, 5.
- [231] N. Bassik, G. M. Stern, M. Jamal, D. H. Gracias, *Adv. Mater.* **2008**, *20*, 4760.
- [232] G. P. Nikishkov, *J. Appl. Phys.* **2003**, *94*, 5333.
- [233] N. Bassik, G. M. Stern, D. H. Gracias, *Appl. Phys. Lett.* **2009**, *95*, 091901.
- [234] P. O. Vaccaro, K. Kubota, T. Fleischmann, S. Saravanan, T. Aida, *Microelectron. J.* **2003**, *34*, 447.
- [235] P. Tyagi, N. Bassik, T. G. Leong, J. H. Cho, B. R. Benson, D. H. Gracias, *J. Microelectromech. Syst.* **2009**, *18*, 784.
- [236] I. Stewart, *Nature* **2007**, *448*, 419.
- [237] T. Nojima, K. Saito, *JSME Int. J., Ser. A* **2006**, *49*, 38.
- [238] D. H. Gracias, *Curr. Opin. Chem. Eng.* **2013**, *2*, 112.
- [239] Q. Ge, C. K. Dunn, H. J. Qi, M. L. Dunn, *Smart Mater. Struct.* **2014**, *23*, 094007.
- [240] S. Tibbets, *Archit. Des.* **2014**, *84*, 116.
- [241] B. G. Compton, J. A. Lewis, *Adv. Mater.* **2014**, *26*, 5930.
- [242] K. Haraguchi, T. Takehisa, *Adv. Mater.* **2002**, *14*, 1120.
- [243] S. Armon, E. Efrati, R. Kupferman, E. Sharon, *Science* **2011**, *333*, 1726.
- [244] H. Aharoni, E. Sharon, R. Kupferman, *Phys. Rev. Lett.* **2014**, *113*, 257801.
- [245] D. Ratna, J. Karger-Kocsis, *J. Mater. Sci.* **2008**, *43*, 254.
- [246] J. Wu, C. Yuan, Z. Ding, M. Isakov, Y. Mao, T. Wang, M. L. Dunn, H. J. Qi, *Sci. Rep.* **2016**, *6*, 24224.
- [247] Q. Ge, H. J. Qi, M. L. Dunn, *Appl. Phys. Lett.* **2013**, *103*, 131901.
- [248] W. Li, G. Huang, H. Yan, J. Wang, Y. Yu, X. Hu, X. Wu, Y. Mei, *Soft Matter* **2012**, *8*, 7103.
- [249] T. G. Leong, C. L. Randall, B. R. Benson, N. Bassik, G. M. Stern, D. H. Gracias, *Proc. Natl. Acad. Sci. USA* **2009**, *106*, 703.
- [250] K. Kobayashi, S. H. Oh, C. K. Yoon, D. H. Gracias, *Macromol. Rapid Commun.* **2018**, *39*, 1700692.
- [251] S. Han, M. Hagiwara, T. Ishizone, *Macromolecules* **2003**, *36*, 8312.
- [252] J. F. Lutz, *J. Polym. Sci., Part A: Polym. Chem.* **2008**, *46*, 3459.
- [253] C. Ye, S. V. Nikolov, R. Calabrese, A. Dindar, A. Alexeev, B. Kippelen, D. L. Kaplan, V. V. Tsukruk, *Angew. Chem., Int. Ed.* **2015**, *54*, 8490.
- [254] X. Zhang, C. L. Pint, M. H. Lee, B. E. Schubert, A. Jamshidi, K. Takei, H. Ko, A. Gillies, R. Bardhan, J. J. Urban, M. Wu, R. Fearing, A. Javey, *Nano Lett.* **2011**, *11*, 3239.
- [255] S. M. Bachilo, M. S. Strano, C. Kittrell, R. H. Hauge, R. E. Smalley, R. B. Weisman, *Science* **2002**, *298*, 2361.
- [256] M. O'connell, S. Bachilo, C. Huffman, *Science* **2002**, *297*, 593.
- [257] Y. Yu, M. Nakano, T. Ikeda, *Nature* **2003**, *425*, 145.
- [258] K. S. Novoselov, A. Mishchenko, A. Carvalho, A. H. C. Neto, *Science* **2016**, *353*, aac9439.
- [259] A. K. Geim, I. V. Grigorieva, *Nature* **2013**, *499*, 419.
- [260] Y. Liu, N. O. Weiss, X. Duan, H.-C. Cheng, Y. Huang, X. Duan, *Nat. Rev. Mater.* **2016**, *1*, 16042.
- [261] D. Jariwala, T. J. Marks, M. C. Hersam, *Nat. Mater.* **2017**, *16*, 170.